

# Travertine records climate-induced transformations of the Yellowstone hydrothermal system from the late Pleistocene to the present

Lauren N. Harrison<sup>1,2,†</sup>, Shaul Hurwitz<sup>2</sup>, James B. Paces<sup>3</sup>, Cathy Whitlock<sup>4</sup>, Sara Peek<sup>2</sup>, and Joseph Licciardi<sup>5</sup>

<sup>1</sup>Department of Geosciences, Colorado State University, 1482 Campus Delivery, Fort Collins, Colorado 80523-1482, USA

<sup>2</sup>Volcano Science Center, U.S. Geological Survey, 350 N. Akron Road, Moffett Field, California 94035, USA

<sup>3</sup>Denver Federal Center, U.S. Geological Survey, P.O. Box 25046, MS 980, Lakewood, Colorado 80225, USA

<sup>4</sup>Department of Earth Sciences, Montana State University, Leon Johnson Hall 710, Bozeman, Montana 59715, USA

<sup>5</sup>Department of Earth Sciences, University of New Hampshire, James Hall 214, Durham, New Hampshire 03824, USA

## ABSTRACT

Chemical changes in hot springs, as recorded by thermal waters and their deposits, provide a window into the evolution of the postglacial hydrothermal system of the Yellowstone Plateau Volcanic Field. Today, most hydrothermal travertine forms to the north and south of the ca. 631 ka Yellowstone caldera where groundwater flow through subsurface sedimentary rocks leads to calcite saturation at hot springs. In contrast, low-Ca rhyolites dominate the subsurface within the Yellowstone caldera, resulting in thermal waters that rarely deposit travertine. We investigated the timing and origin of five small travertine deposits in the Upper and Lower Geyser Basins to understand the conditions that allowed for travertine deposition. New <sup>230</sup>Th-U dating, oxygen ( $\delta^{18}\text{O}$ ), carbon ( $\delta^{13}\text{C}$ ), and strontium ( $^{87}\text{Sr}/^{86}\text{Sr}$ ) isotopic ratios, and elemental concentrations indicate that travertine deposits within the Yellowstone caldera formed during three main episodes that correspond broadly with known periods of wet climate: 13.9–13.6 ka, 12.2–9.5 ka, and 5.2–2.9 ka. Travertine deposition occurred in response to the influx of large volumes of cold meteoric water, which increased the rate of chemical weathering of surficial sediments and recharge into the hydrothermal system. The small volume of intracaldera travertine does not support a massive postglacial surge of  $\text{CO}_2$  within the Yellowstone caldera, nor was magmatic  $\text{CO}_2$  the catalyst for postglacial travertine deposition.


## INTRODUCTION

Volcano-hydrothermal systems evolve over time in direct response to magmatic, tectonic, and climatic forcing mechanisms that dictate rates of water recharge, thermal fluid circulation patterns, and thermal dissipation. Understanding the factors that are the most influential in active, unexhumed hydrothermal systems is often difficult without a temporal perspective on how the system responded to known internal and external forces. Fortunately, the chemistry of thermal waters and their mineral deposits provide a window into the evolution of hydrothermal systems (Hurwitz and Lowenstern, 2014, and references therein). The location, volume, and deposition rate of travertine provide a record of hydrothermal changes over annual to millennial time scales since the late Pleistocene (Fig. 1; Berger, 1978; Sturchio et al., 1994; Fouke et al., 2000; Fouke, 2011; Chafetz and Guidry, 2003; De Boever et al., 2022). The most well-known and studied travertine deposit in Yellowstone National Park is at Mammoth Hot Springs (Bargar, 1978; Pierce et al., 1991), but travertine has also been deposited within the Yellowstone caldera in the Upper and Lower Geyser Basins and near the southern boundary of Yellowstone National Park (Fig. 1).

Small travertine deposits (<50 m in length and only several meters high) within the Yellowstone caldera are associated with thermal springs that are not currently depositing travertine or are extinct. The subsurface within the Yellowstone caldera consists of thick rhyolite flows and ignimbrites that are poor in calcium (Christiansen, 2001), so thermal waters discharging at hot springs are mostly near saturation with respect to silica ( $\text{SiO}_2$ ), not calcium carbonate. The existence of travertine within the caldera, therefore,

is puzzling and requires hydrochemical conditions that are not presently typical for the major intracaldera geyser basins.

Mechanisms driving past travertine deposition within the Yellowstone caldera could have originated at either shallower or deeper levels within the hydrothermal system (Fig. 2). A potential shallow mechanism could have been large influxes of cold meteoric water into the hydrothermal system that cooled groundwater temperatures and increased calcium concentrations. This meteoric water could have originated as meltwater from Pinedale glaciers, which at their maximum extent from 22 ka to 14.5 ka covered the Yellowstone Plateau in over 1 km of ice (Bargar and Fournier, 1988; Licciardi and Pierce, 2018), or as rainfall during prolonged wet periods (centennial to millennial scale in duration; Fig. 2A). Alternatively, travertine deposition may have been catalyzed by the release of subsurface carbon dioxide, either from postglacial crustal decompression, seismic events releasing accumulated crustal volatiles (Fig. 2B), or degassing of shallow (<5 km depth) magmatic intrusions (Fig. 2C). As there have been no known volcanic eruptions since ca. 70 ka (Christiansen, 2001; Stelten et al., 2023), localized spikes in  $\text{CO}_2$  from magmatic degassing of shallow intrusions (<5 km depth) are ruled out. Therefore, the timing of hydrothermal travertine deposition within the Yellowstone caldera is related to postglacial climate and/or the occurrence of past seismic events. This study used <sup>230</sup>Th-U ages, isotopic compositions of carbon ( $\delta^{13}\text{C}$ ), oxygen ( $\delta^{18}\text{O}$ ), and strontium ( $^{87}\text{Sr}/^{86}\text{Sr}$ ), and the elemental compositions of travertine deposits within the Yellowstone caldera to understand the role of different external forces in triggering deposition of these unique intracaldera travertine deposits.

Lauren N. Harrison  <https://orcid.org/0000-0002-6621-5958>

<sup>†</sup>lauren.n.harrison@colostate.edu

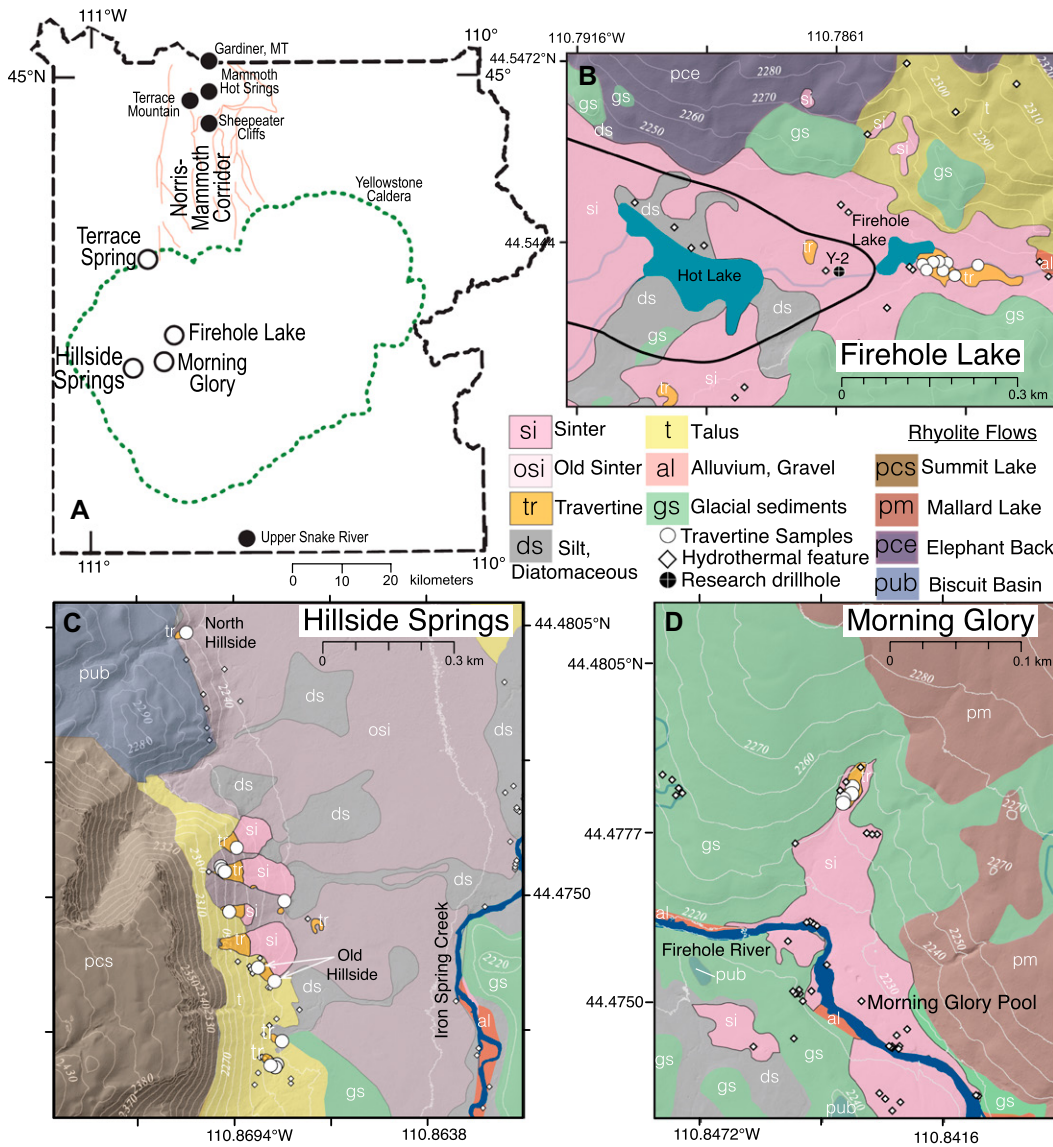


**Figure 1.** (A) Map of the locations of travertine deposits within Yellowstone National Park (the black dashed line is the boundary of Yellowstone National Park). Open circles labeled with large font indicate intracaldera travertine deposits investigated in this study. Filled circles labeled with small font indicate other travertine areas in Yellowstone National Park not included in this study. Green dotted outline indicates the most recent (ca. 631 ka) caldera, and orange lines denote the fault zone that delineates the Norris-Mammoth corridor. (B–D) Lithostratigraphic units draped onto topography, the locations of travertine samples, and active hydrothermal features. Background on these figures is 2020 light detection and ranging (LiDAR) data (U.S. Geological Survey 3D Elevation Program, 2022) and geologic contacts (Waldrop and Pierce, 1975; Muffler et al., 1982a, 1982b; Christiansen, 2001). (B) Firehole Lake, Lower Geyser Basin. (C) Hillside Springs Group, Upper Geyser Basin. (D) Travertine near Morning Glory Pool, Upper Geyser Basin. See Figure S1 for a map of Terrace Spring, descriptions of travertine samples, and field photographs (see text footnote 1).

**GEOLOGY AND STUDY REGION**

The term travertine in this study refers to nonmarine carbonates (CaCO<sub>3</sub> as calcite and aragonite) precipitated from groundwater discharged at thermal springs (Fouke et al., 2000). In the Yellowstone hydrothermal system, circulating groundwater is heated by the magmatic system; rises along crustal faults and permeable zones such as the edges of rhyolite flows, where it may mix with cool meteoric water or boil; and discharges at hot springs (Fournier, 1989; Hurwitz and Lowenstern, 2014). Upon discharge, reductions in both pressure and temperature result in exsolution of dissolved CO<sub>2</sub>, supersaturating waters with carbonate species and triggering mineral precipitation (Friedman, 1970). Modern travertine-

depositing waters in Mammoth Hot Springs discharge at temperatures of ~70 °C, which is below the boiling point of pure water for their elevations (92–94 °C). The source of calcium and carbonate at Mammoth Hot Springs originates from the dissolution of Paleozoic and Mesozoic limestones and evaporites in the subsurface (Pierce et al., 1991). The travertine deposits described in this study are within the ca. 631 ka Yellowstone caldera and are located in the Upper Geyser Basin (near Morning Glory Pool and the Hillside Springs Group), the Lower Geyser Basin (east of Firehole Lake), and at Terrace Spring near Madison Junction (Fig. 1; Waldrop and Pierce, 1975; Waldrop, 1975; Muffler et al., 1982a, 1982b). These deposits precipitated subaerially, supported by the ubiquitous presence of finely laminated

beds (rather than the poor bedding typically found in tufas) and the large crystal size and euhedral habit (shrubs, spars, dendrites, blades, or shards) of carbonate grains (Capezzuoli et al., 2014). Present-day climate in the Upper and Lower Geyser Basins is best approximated using the Old Faithful climate station, where the records span from 1904 to the present (<https://wrcc.dri.edu/cgi-bin/cliMAIN.pl?wy6845>, accessed March 2023). Average temperatures over the period of record are -9.8 °C in January, 14.0 °C in July, and 1.3 °C annually. Precipitation is high in December–January and May–June. Much of the precipitation falls as snow (November–March), while summers (July–September) are relatively dry. The highest discharge in the Firehole River (whose catchment includes all the Upper and

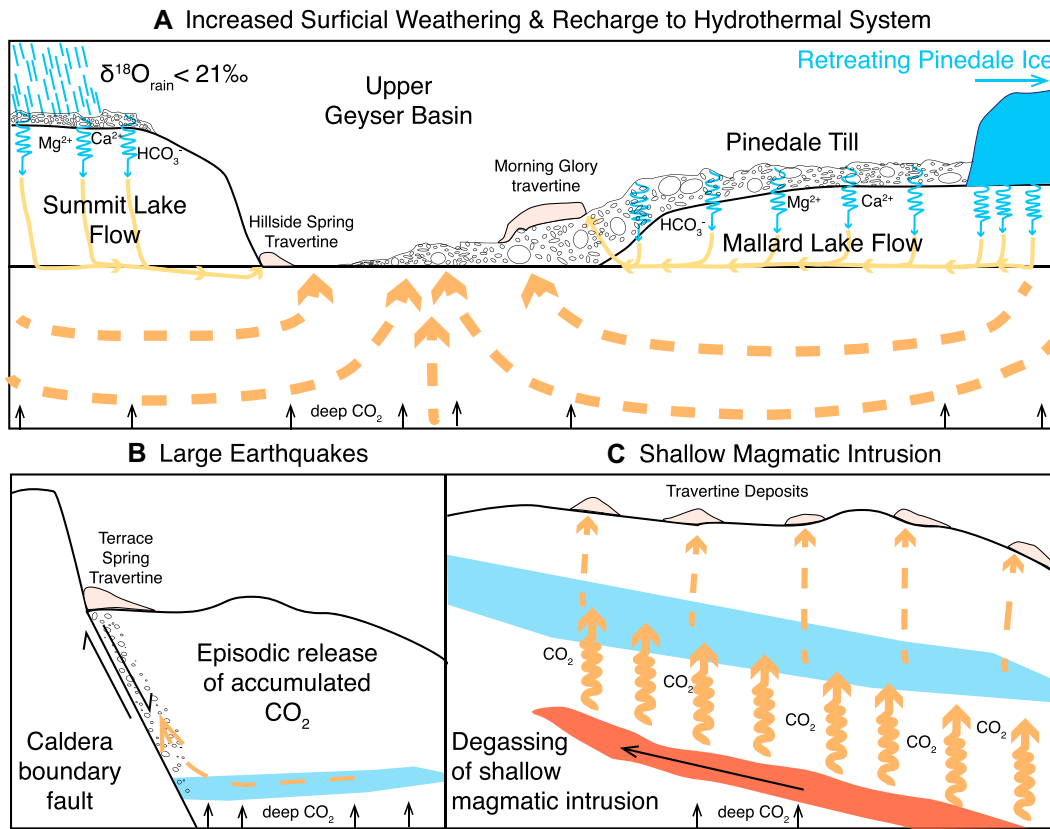


**Figure 2.** Cartoons illustrating different potential deposition mechanisms of within-caldera travertine discussed in the text. Blue arrows indicate cold meteoric water infiltration, large dark orange arrows indicate hot thermal water upwelling zones, and thin light orange arrows indicate lower-temperature thermal waters with shallower flow paths than the main upflow zones. Note that the flux of deep CO<sub>2</sub> from the Yellowstone deep magmatic reservoir (~5–17 km depth) is portrayed as constant from the late Pleistocene to the present for all scenarios. (A) Increased weathering of surficial sediments and recharge to the hydrothermal system during deglaciation or periods of high precipitation. The increased availability of fresh glacial tills composed of glacially transported rocks (basalts, andesites, and dacites) from the eastern Yellowstone region provide critical sources

of Ca<sup>2+</sup>, Mg<sup>2+</sup>, and HCO<sub>3</sub><sup>-</sup> to the hydrothermal system; the rate of weathering of these surficial sediments increases during periods of wet climatic conditions. (B) Release of accumulated volatiles (mostly CO<sub>2</sub>) by earthquakes from previously hydrothermally sealed subsurface. Volatile release is highest in locations above large faults, like Terrace Spring, which is located at the convergence of the Mammoth-Norris fault corridor and the ca. 631 ka caldera rim fault. (C) Offgassing of a magmatic intrusion (here illustrated as a shallow dike, <5 km depth) can result in large travertine deposits that are spatially constrained to locations above the dike intrusion; as there have been no known volcanic eruptions in the Yellowstone Plateau Volcanic Field since ca. 70 ka, we rule this out as a potential mechanism for the formation of within-caldera travertine.

Lower Geyser Basins) occurs in May and June from the melting of winter snowpack.

#### Firehole Lake Travertine, Lower Geyser Basin

Firehole Lake (2250 meters above sea level [masl]) is located on the far eastern side of the Lower Geyser Basin in a narrow valley between the Mallard Lake and Elephant Back rhyolite flows (Fig. 1B; Fig. S5 in the Supplemental Material<sup>1</sup>). Several hot springs are currently active on the banks of Firehole Lake, which is itself a thermal feature. The travertine deposit is east of these active features and forms a wide low-relief, flat-topped set of terraces that cover

an area roughly 185 m by 60 m. The travertine in many spots is brown from coprecipitation of manganese oxides and carbonates with the travertine, and in some locations, thin layers of calcite are interspersed with thin layers of manganese oxides and carbonates. The exposed section of the deposit is estimated to be ~3.3 m thick.

#### Hillside Springs Travertine, Upper Geyser Basin

The Hillside Springs Group is an active set of springs that discharge from the Summit Lake rhyolite flow; they are the westernmost springs in the Upper Geyser Basin (Fig. 1C; Fig. S2). The springs issue from high on a hillside (2280 masl) and have deposited both carbonate and silica minerals, although they do not precipitate appreciable amounts of either mineral at present (Allen and Day, 1935). Large outcrops of older travertine can be found below (2234–2264 masl) the currently active springs, where they form

dissected and eroded mound- and fissure-type structures of low relief. The exposed thickness of these deposits is less than 4 m. An isolated spring ~500 m northwest of the main Hillside Springs Group actively discharges at 2251 masl and is associated with another deposit of travertine (Fig. S3). The mound here is 4 m wide by 2.5 m high and exhibits a transition from layers exclusively composed of 0.5- to 2-cm-thick travertine to the top meter exhibiting interlayered silica sinter and travertine.

#### Travertine near Morning Glory Pool, Upper Geyser Basin

Travertine deposits in a small draw ~400 m north of Morning Glory Pool (2247 masl) on the east side of the Upper Geyser Basin form a single low, flat-topped terrace that is not associated with any active thermal springs (Fig. 1D; Fig. S4). This travertine deposit is roughly 53 m by 22 m in size, centered within a drainage where

<sup>1</sup>Supplemental Material. Field photos of all travertine deposits described in this manuscript and a geologic map of Terrace Spring. Please visit <https://doi.org/10.1130/GSAB.S.24891144> to access the supplemental material, and contact editing@geosociety.org with any questions.

paleowaters issued through unconsolidated Pinedale-age glacial till (Waldrop, 1975; Muffler et al., 1982b). The travertine is layered, with prominent, 15-cm- to 30-cm-thick beds of hard, dense travertine alternating with thinner layers a few millimeters to 1.5 cm thick, all of which are buff to pinkish in hue. The exposed thickness is less than 1 m.

### Terrace Spring Travertine, Caldera Boundary

Terrace Spring (2100 masl) is a currently active hot spring pool just north of Madison Junction located at the intersection of the youngest caldera rim fault with major north-south-trending faults of the Norris-Mammoth corridor (Fig. S1). The pool is usually characterized by vigorous bubbling due to the very high flux of CO<sub>2</sub> (Lowenstern et al., 2005) and temperatures below boiling (~50 °C maximum measured in July 2021). Travertine deposits spread out on a wide, low-sloping plain east and downhill of the currently active springs, forming flat terraces, low outcrops dispersed in a grassy field, and small low benches of old terrace cascades. Exposed stratigraphy is estimated to be no more than 0.5 m.

### METHODS

We identified and sampled travertine over three field seasons. Thin sections were cut and examined under plane- and cross-polarized light to identify travertine textures, accessory minerals, and lithics. Small, ~50–100 g pieces of fresh travertine were analyzed for major- and minor-element concentrations using X-ray fluorescence (XRF) on a Perform'X X-ray fluorescence spectrometer at Hamilton Analytical Laboratory at Hamilton College, New York. Fused discs were analyzed for trace-element concentrations using a laser ablation-inductively coupled plasma-mass spectrometer (LA-ICP-MS) at the Colorado School of Mines, Golden, Colorado (detailed methods and data are provided in Harrison et al., 2023).

Rock slabs were cut perpendicular to bedding surfaces and polished to expose fine structures. Small aliquots (40–150 mg) of material from single travertine layers were excavated with a dental drill under a binocular microscope, avoiding areas of diagenetic alteration (e.g., euhedral crystals in voids; recrystallized areas along bedding planes; areas with different fluorescent properties when viewed under shortwave infrared light; see the Supplementary Material [footnote 1]; Harrison et al., 2023) and contamination with detrital material. Aliquots of this powder were analyzed for stable oxygen and carbon

isotope compositions, as well as for strontium, uranium, and thorium isotopes. Oxygen and carbon isotope compositions were measured at the U.S. Geological Survey (USGS) Reston Stable Isotope Laboratory in Reston, Virginia, using standard techniques (method details in Harrison et al., 2023). Oxygen isotope ratios are reported as  $\delta^{18}\text{O}$  relative to Vienna standard mean ocean water (VSMOW) calculated as  $([^{18}\text{O}/^{16}\text{O}]_{\text{sample}}/[^{18}\text{O}/^{16}\text{O}]_{\text{standard}} - 1) \times 1000$  (Coplen, 1994). Carbon isotope results are reported as  $\delta^{13}\text{C}$  relative to Vienna Pee Dee belemnite (VPDB) calculated as  $([^{13}\text{C}/^{12}\text{C}]_{\text{sample}}/[^{13}\text{C}/^{12}\text{C}]_{\text{standard}} - 1) \times 1000$  (Coplen, 1994).

The Th and U isotope dilution measurements were determined on 20–40 mg aliquots of travertine powders at the USGS Denver Radiogenic Isotope Laboratory. Samples were spiked with a high-purity <sup>233</sup>U-<sup>236</sup>U-<sup>229</sup>Th tracer solution prior to hot-plate digestion using ultrapure acids. U and Th were separated and purified on ion exchange columns using Bio-Rad AG1 × 8 anion resin and analyzed on a Thermo-Finnigan Triton multicollector thermal ionization mass spectrometer (TIMS) using peak jumping on a single electron multiplier (for method details, standard values, and measured reference material results, see Paces et al., 2022, and Harrison et al., 2023).

Initial [<sup>234</sup>U/<sup>238</sup>U] values were close to 1 for all samples (mostly 1.02–1.16), similar to values measured in modern thermal waters (1.05–1.07 for Hillside Group Springs, 1.031 for Morning Glory Pool, 1.033 for Terrace Spring; Paces et al., 2022). In addition, uranium isotopic compositions did not correlate with age, and none of the samples had <sup>230</sup>Th-U ages older than the last glacial period (ca. 22–14.5 ka); both findings indicate that significant postdepositional open-system behavior did not occur.

Strontium was separated from the same analytical aliquots as U-series isotopes and purified using Sr-spec resin. Unspiked strontium isotopes were measured on the same multicollector TIMS using triple-jump, multidynamic analyses (Paces et al., 2022; Harrison et al., 2023).

### RESULTS

We report new chemical and isotopic analyses for 63 travertine layers from 30 samples. Data and detailed description of the methods are available in Paces et al. (2022) and Harrison et al. (2023). Most samples, except those near Morning Glory Pool, had [<sup>230</sup>Th/<sup>232</sup>Th] values (square brackets denote activity ratios) greater than 10, which resulted in robust <sup>230</sup>Th-U disequilibrium ages requiring only minimal corrections for common Th (i.e., <sup>232</sup>Th plus associated <sup>230</sup>Th contributed from a nonauthigenic

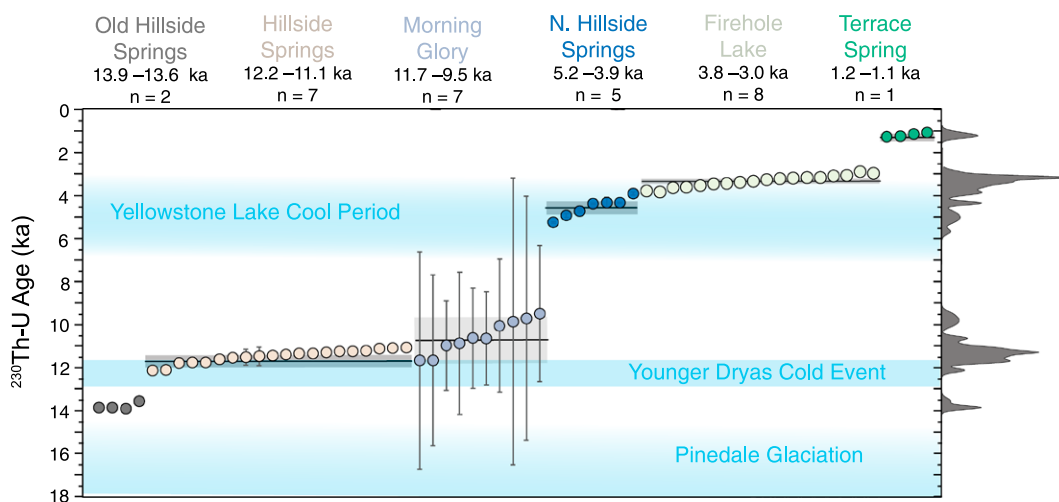
detrital component). Samples from locations near Morning Glory Pool had high concentrations of <sup>232</sup>Th and elements found in detrital silicates (Al, Zr, and chemical index of alteration [CIA] elements), which indicate the deposits incorporated a larger component of silicate dust or dissolved salts during their formation relative to other travertines in this study. Because some of the <sup>230</sup>Th present in travertines with elevated <sup>232</sup>Th is exogenous and not supported by radiogenic decay of uranium present in the samples, <sup>230</sup>Th contributions from the detrital component must be mathematically subtracted from the analysis; this treatment resulted in larger uncertainties in <sup>230</sup>Th-U ages (Ludwig and Paces, 2002).

The <sup>230</sup>Th-U age results showed three main episodes of travertine deposition within the Yellowstone caldera (Fig. 3). The first interval occurred between 13.9 ka and 13.6 ka, soon after recession of Pinedale glaciers, and is recorded in the stratigraphically deepest deposits at Hillside Springs. Following this, a major period of deposition occurred from 12.2 ka to 9.5 ka at Hillside Springs and near Morning Glory Pool, followed by an ~4 k.y. hiatus during much of the early Holocene. Travertine precipitation ceased completely at the main Hillside Springs and near Morning Glory Pool after the second depositional episode, but late Holocene precipitation occurred at north Hillside between 5.2 ka and 3.9 ka, followed closely by travertine deposition near Firehole Lake from 3.8 ka to 3.0 ka. The veneer of travertine deposited near Terrace Spring is ca. 1.2 ka.

The Hillside Springs travertines are divided into three groups (Old Hillside, Hillside, and north Hillside) that are spatially and temporally distinct (Fig. 1C). The Old Hillside Springs travertines have ages older than 13.5 ka and are stratigraphically the deepest. The main Hillside Springs deposit forms a continuous stratigraphic section best exposed at the southernmost end of the thermal area and has ages between 12.2 ka and 11.1 ka. An isolated thermal feature and travertine deposit at north Hillside (0.5 km north of the other Hillside Springs thermal features) formed between 5.2 ka and 3.9 ka and has no exposed travertines that correlate with the older Hillside Springs deposits.

Travertine deposits from different locations and ages tend to cluster into groups with similar strontium and oxygen isotopic compositions (Figs. 4 and 5). Travertine <sup>87</sup>Sr/<sup>86</sup>Sr values vary between 0.70979 and 0.71079 and do not show obvious temporal trends. Instead, samples from different locations tend to have similar <sup>87</sup>Sr/<sup>86</sup>Sr ratios that cluster over narrow and distinct ranges (Fig. 5). The  $\delta^{18}\text{O}$  values vary between  $-1.25\text{‰}$  and  $9.37\text{‰}$ , with older travertines broadly exhib-





shown on top of the diagram, where  $n$  is the number of travertine samples of that age (points on the plot denote different analytical aliquots, some of which are different travertine layers from the same sample).

**Figure 3.** Uranium-series ( $^{230}\text{Th}$ -U) ages for travertines. Blue fields designate relevant climatic events: the latest stage of Pinedale glaciation (Licciardi and Pierce, 2018), the Younger Dryas cold event (Cheng et al., 2020), and the cool climatic episode identified in Yellowstone Lake sediment cores (Brown et al., 2021). The histogram on the right side of the diagram is a kernel density estimate of U-series ages, illustrating periods of high travertine deposition. The ages and errors for each travertine group discussed in the text are

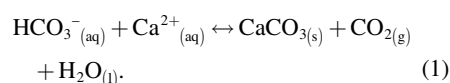
iting lower  $\delta^{18}\text{O}$  values and younger travertines exhibiting higher values (Fig. 4). Similarly, older travertines have higher relative magnesium content and CIA values than younger travertines (Fig. 6). CIA is defined as  $\text{CIA} = [\text{Al}_2\text{O}_3 / (\text{Al}_2\text{O}_3 + \text{CaO}^* + \text{Na}_2\text{O} + \text{K}_2\text{O})] \times 100$ , where all oxides are calculated as molar oxides, and  $\text{CaO}^*$  is calcium oxide in the silicate fraction only, here calculated using  $\text{CaO} = \text{Na}_2\text{O}$ . In this study, CIA was used as an indication of removal of mobile cations from surficial sediments during chemical weathering, facilitated by the high chemical weathering that accompanied the transition from glacial to interglacial epochs (Wang et al., 2020). The  $\delta^{13}\text{C}$  values vary between  $-0.70\%$  and  $4.23\%$ ; travertines from different locations tend to cluster around similar values (Fig. 4).

## DISCUSSION

### Controls on Travertine Deposition in the Yellowstone Hydrothermal System

Sources of bicarbonate and calcium are necessary for travertine deposition. There are several sources of  $\text{CO}_2$ , and therefore bicarbonate, to the Yellowstone hydrothermal system. One source is basaltic magma deep within the crust and subsequent crystallization of more evolved magma bodies at shallower crustal levels (e.g., long-lived magma reservoirs between  $\sim 5$  km and 17 km depth; Fournier, 1989; Werner and Brantley, 2003; Moran et al., 2017). Another possible source is from decomposition of carbonate-rich sedimentary rock underlying Quaternary volcanic units, although limestones originally beneath the present-day caldera have likely been at least partially consumed during the 2.2 m.y. life-

time of Yellowstone volcanism (Christiansen, 2001; Lowenstern et al., 2015). Another possible source of  $\text{CO}_2$  is decomposition of organic material; however, within the Upper and Lower Geyser Basins, input of  $\text{CO}_2$  from biotic sources is assumed to be negligible based on ratios of  $\text{CH}_4$  to higher-order organic compounds (i.e., ethane, propane, butane, etc.), which are less than 1000 in fumarole gases (Bergfeld et al., 2014; Moran et al., 2017). Regardless of where  $\text{CO}_2$  originates, the hydrothermal system buffers inputs of deep  $\text{CO}_2$  by dissolution into thermal fluids and precipitation of secondary minerals in the deep subsurface during steam separation via the generalized reaction:



The deposition of travertine at the surface occurs when  $\text{CO}_2$  exsolves from groundwater due to a reduction in the partial pressure of  $\text{CO}_2$  ( $p\text{CO}_2$ ) as spring discharge approaches atmospheric pressure. Temperature, pH, and the concentrations of  $\text{Ca}^{2+}$ ,  $\text{Mg}^{2+}$ ,  $\text{HCO}_3^-$ , and  $\text{SO}_4^{2-}$  are likely important parameters controlling the precipitation of the calcium carbonate ( $\text{CaCO}_3$ ) minerals in travertine deposits (Luo et al., 2022). The concentrations of Ca and Mg in the alkaline waters of the geyser basins today are typically less than 1 mg/L and 0.05 mg/L, respectively (McCleskey et al., 2022), and are too low for carbonate saturation. The travertine deposits investigated in this study are located at the margins of the Upper and Lower Geyser Basins, where spring temperatures are typically below

boiling, the concentrations of  $\text{Ca}^{2+}$  and  $\text{Mg}^{2+}$  are slightly higher, the  $\text{Cl}^-$  and  $\text{SiO}_2$  concentrations are lower, and the  $\text{HCO}_3^-$  concentrations are comparable to or higher than those in the central parts of the basins, where most springs discharge at boiling temperature.

The postglacial episodes of intracaldera travertine deposition most likely resulted from either higher  $\text{CO}_2$  concentrations (as bicarbonate,  $\text{HCO}_3^-$ ) or higher  $\text{Ca}^{2+}$  and  $\text{Mg}^{2+}$  concentrations, or both, in paleo-groundwater compared with concentrations in modern groundwater. Increases in  $\text{CO}_2$  into the deep hydrothermal system would have driven dissolution of calcite at depth and resulted in higher concentrations of  $\text{Ca}^{2+}$  and  $\text{HCO}_3^-$  in thermal waters according to Equation 1. This increased flux could have originated from concurrent shallow degassing of basaltic intrusions, as has been hypothesized on the Colorado Plateau (Priewisch et al., 2014). However, there is no evidence for late Pleistocene shallow ( $< 5$  km depth) basaltic magma intrusions in the Yellowstone Plateau Volcanic Field (Christiansen, 2001), nor is there evidence for large deposits of travertine that would have been produced by such intrusion(s) (see ‘‘Travertine Deposit Volume and  $\text{CO}_2$  Flux’’ section below). Instead, pulses of travertine deposition likely track greater influxes of  $\text{Ca}^{2+}$  and  $\text{Mg}^{2+}$  into the hydrothermal system.

Pinedale ice recession was well under way in the northern, eastern, and southern parts of the region from 18 ka to 14.5 ka, based on the ages of moraines around Yellowstone Plateau (Fig. 7B; Licciardi and Pierce, 2018). The melting of the  $\sim 1$ -km-thick Yellowstone ice cap would have produced large volumes

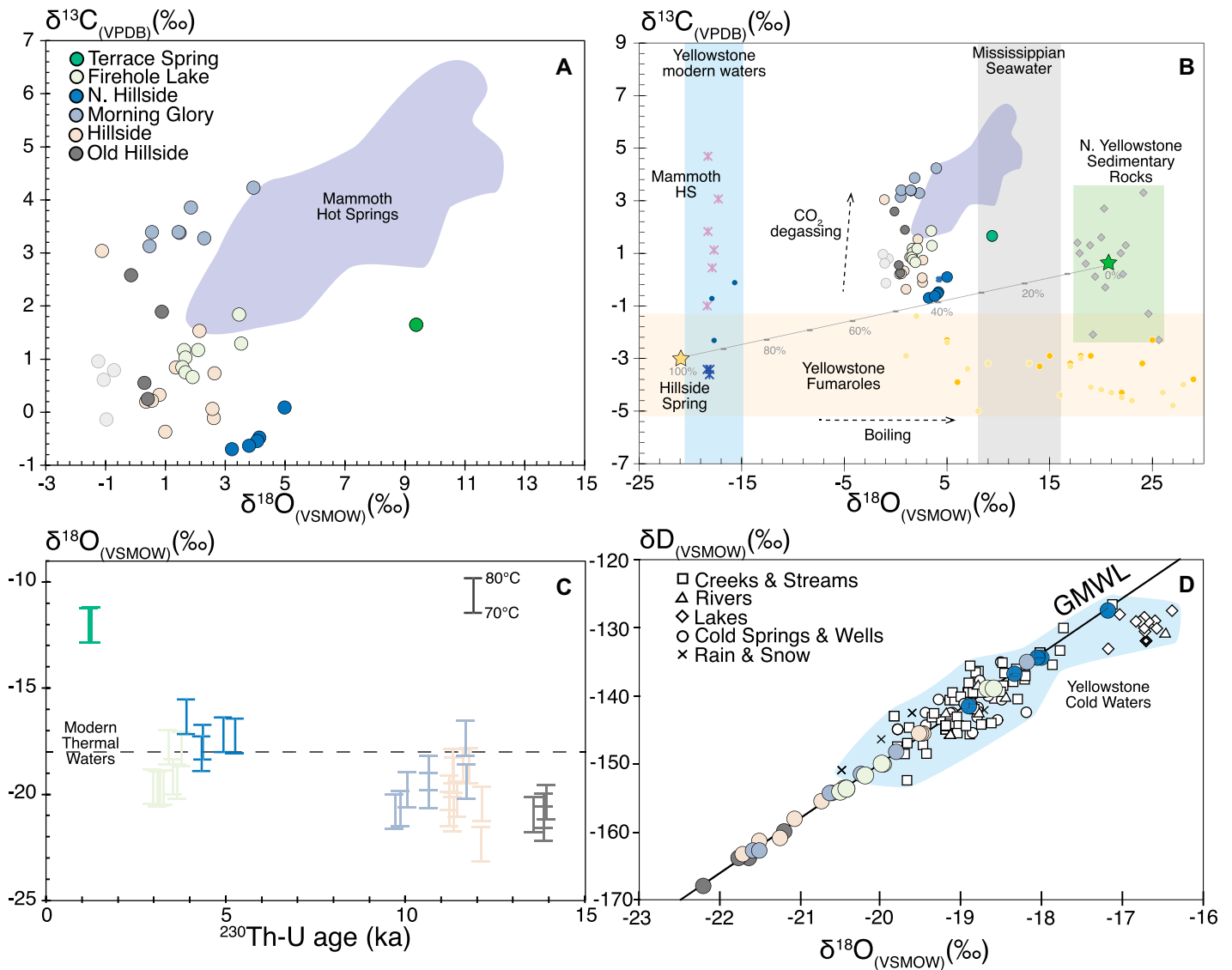


**Figure 4.** Stable isotope composition of Yellowstone hydrothermal travertines and other materials. (A and B)  $\delta^{18}\text{O}$  (‰, Vienna standard mean ocean water [VSMOW]) and  $\delta^{13}\text{C}$  (‰, Vienna Pee Dee belemnite [VPDB]) of (A) Yellowstone hydrothermal travertines from this study compared to those from Mammoth Hot Springs (HS) and (B) Yellowstone hydrothermal travertines and related reservoirs. Error bars are smaller than the data points on both plots ( $\pm 0.2\text{‰}$  for both  $\delta^{18}\text{O}_{\text{carbonate}}$  and  $\delta^{13}\text{C}_{\text{carbonate}}$ ). Data for Mammoth Hot Springs travertine are from Fouke et al. (2000), Friedman (1970), Chafetz and Lawrence (1994), De Boever et al. (2022), and Chafetz and Guidry (2003). Legend in part A applies to the entire figure. In part B, the range of  $\delta^{18}\text{O}_{\text{water}}$  for modern Yellowstone cold waters (light-blue vertical band) is from Kharaka et al. (2002). Compositions of individual water samples from the Hillside Springs Group and Mammoth Hot Springs are shown with asterisk symbols (data from McCleskey et al., 2022; Fouke et al., 2000, respectively). Yellowstone Plateau Volcanic Field  $\delta^{13}\text{C}_{\text{gas}}$  values measured in fumarole gas by Bergfeld et al. (2019) are yellow circles used to define the yellow horizontal band. Values of  $\delta^{18}\text{O}_{\text{water}}$  and  $\delta^{13}\text{C}_{\text{water}}$  in thermal waters ( $\delta^{13}\text{C}$  measured from dissolved inorganic carbon) are shown as orange circles and all plot within the fumarole band. Data for northern Yellowstone region sedimentary rocks (from Friedman, 1970; Kharaka et al., 1991) include carbonate-bearing limestones and evaporites of the Madison Formation and are shown as gray diamonds within a light-green box. For comparison, the range of  $\delta^{18}\text{O}_{\text{seawater}}$  in Mississippian seawater is shown as a vertical gray band. Simple isotopic mixing between average Paleozoic and Mesozoic sedimentary rocks ( $\delta^{18}\text{O}_{\text{av sed}} \approx +21\text{‰}$  and  $\delta^{13}\text{C}_{\text{av sed}} \approx -0.6\text{‰}$ , exposed and sampled north of Yellowstone National Park; Friedman, 1970) and average magmatic gas as approximated by fumarole compositions ( $\delta^{18}\text{O}_{\text{av gas}} \approx -21\text{‰}$  and  $\delta^{13}\text{C}_{\text{av gas}} \approx -3\text{‰}$ ) is shown by the gray line with tick marks at 10% intervals (average values of end members used in the calculation are shown with star symbols). Subsurface boiling will drive thermal fluids to the right on the diagram (dashed boiling line), whereas rapid kinetic fractionation with subaerial  $\text{CO}_2$  degassing will drive waters vertically on the diagram ( $\text{CO}_2$  degassing dashed line). It is possible that the within-caldera travertines were formed by mixing between magmatic  $\text{CO}_2$  and dissolution of Paleozoic and Mesozoic sedimentary rocks in the subsurface followed by rapid  $\text{CO}_2$  degassing, or thermal water boiling followed by rapid  $\text{CO}_2$  degassing, or a combination of the two. (C) Range of  $\delta^{18}\text{O}_{\text{water}}$  calculated to be in equilibrium with the measured  $\delta^{18}\text{O}_{\text{carbonate}}$  at 70 °C and 80 °C (using the equation of Kele et al., 2015). Values falling below the mean

$\delta^{18}\text{O}_{\text{water}}$  for modern thermal waters (dashed horizontal line) illustrate that sources of late Pleistocene and early Holocene groundwater had lower  $\delta^{18}\text{O}_{\text{water}}$ , consistent with glacial meltwater and cool climate precipitation recharging aquifers during that time. (D) Calculated  $\delta^{18}\text{O}_{\text{waters}}$  at 80 °C from part C plotted along the global meteoric water line (GMWL), illustrating the likely predicted oxygen and deuterium values of recharge waters into the hydrothermal system at the time of different travertine deposition. Compositions of modern Yellowstone cold waters are plotted for context (data from Rye and Truesdell, 2007) and outlined in the blue shaded field.

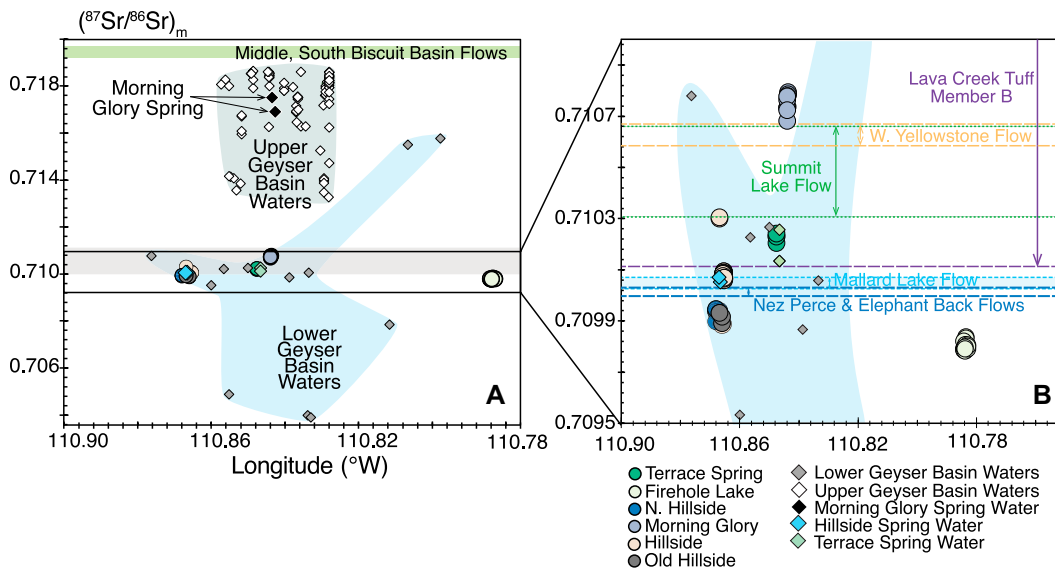


**Figure 5.** Present-day measured strontium isotope composition (not age corrected) of travertines, aquifer rocks, and groundwaters plotted by longitude. (A) Travertine data relative to modern groundwaters discharging in Upper and Lower Geyser Basins and the rocks underlying or adjacent to those basins. The upper and lower bounds for each rhyolite or tuff unit are given as horizontal lines that represent the range of measured  $^{87}\text{Sr}/^{86}\text{Sr}$  values for those units. The horizontal green band is the range of the Middle and South Biscuit Basin flows, and the horizontal gray band is the combined

range of  $^{87}\text{Sr}/^{86}\text{Sr}$  observed in Lava Creek Tuff member B, West Yellowstone flow, Mallard Lake flow, Summit Lake flow, Elephant Back flow, and Nez Perce flow. (B) Enlarged version of travertine data and the ranges of  $^{87}\text{Sr}/^{86}\text{Sr}$  for the latter group of flows. Water data are from Paces et al. (2022). Yellowstone rock data are from Paces et al. (2022), Harrison et al. (2022), Vazquez and Reid (2002), Watts et al. (2012), and Hildreth et al. (1991). Error bars (95% confidence) are smaller than the points.

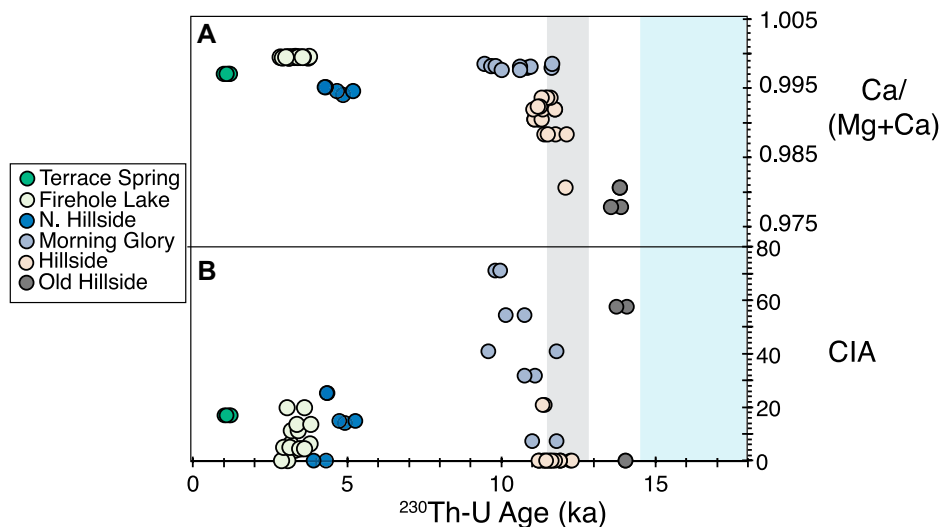


**Figure 6.** Chemical compositions of Yellowstone intracaldera travertines plotted against their  $^{230}\text{Th-U}$  age. (A)  $\text{Ca}/(\text{Mg} + \text{Ca})$  versus  $^{230}\text{Th-U}$  age. (B) CIA (chemical index of alteration) versus  $^{230}\text{Th-U}$  age, with  $\text{CIA} = [\text{Al}_2\text{O}_3/(\text{Al}_2\text{O}_3 + \text{CaO}^* + \text{Na}_2\text{O} + \text{K}_2\text{O})] \times 100$ , where all oxides are calculated as molar oxides, and  $\text{CaO}^*$  is calcium oxide in the silicate fraction only, here calculated using  $\text{CaO} = \text{Na}_2\text{O}$ . Blue field designates the latest stage of Pinedale glaciation, and gray field designates the Younger Dryas cold event (Cheng et al., 2020).

of water charged with high total dissolved solids due to supercharged rates of silicate weathering driven by the production of highly particle-reactive glacial flours and sediments (Wang et al., 2020). This geochemical signature is observed as elevated Mg concentrations in the oldest, ca. 14 ka travertine deposits (Fig. 6A). The influx of meltwater into the shallow hydrothermal system would have lowered water temperatures in addition to providing additional  $\text{Ca}^{2+}$ . Lower temperatures of groundwater in the shallow hydrothermal system would have suppressed subsurface thermal fluid boiling and associated loss of gaseous  $\text{CO}_2$ . Consequently, the equilibrium in Equation 1 would have been driven toward the left, resulting in decreased calcite precipitation and sequestration of calcium in the subsurface. Cooler temperatures also would have increased the reactivity of thermal waters with subsurface rhyolite flows, which is more effective at temperatures below 275 °C, further boosting calcium concentrations in discharging thermal waters (Bischoff and Rosenbauer, 1996; Cullen et al., 2019).

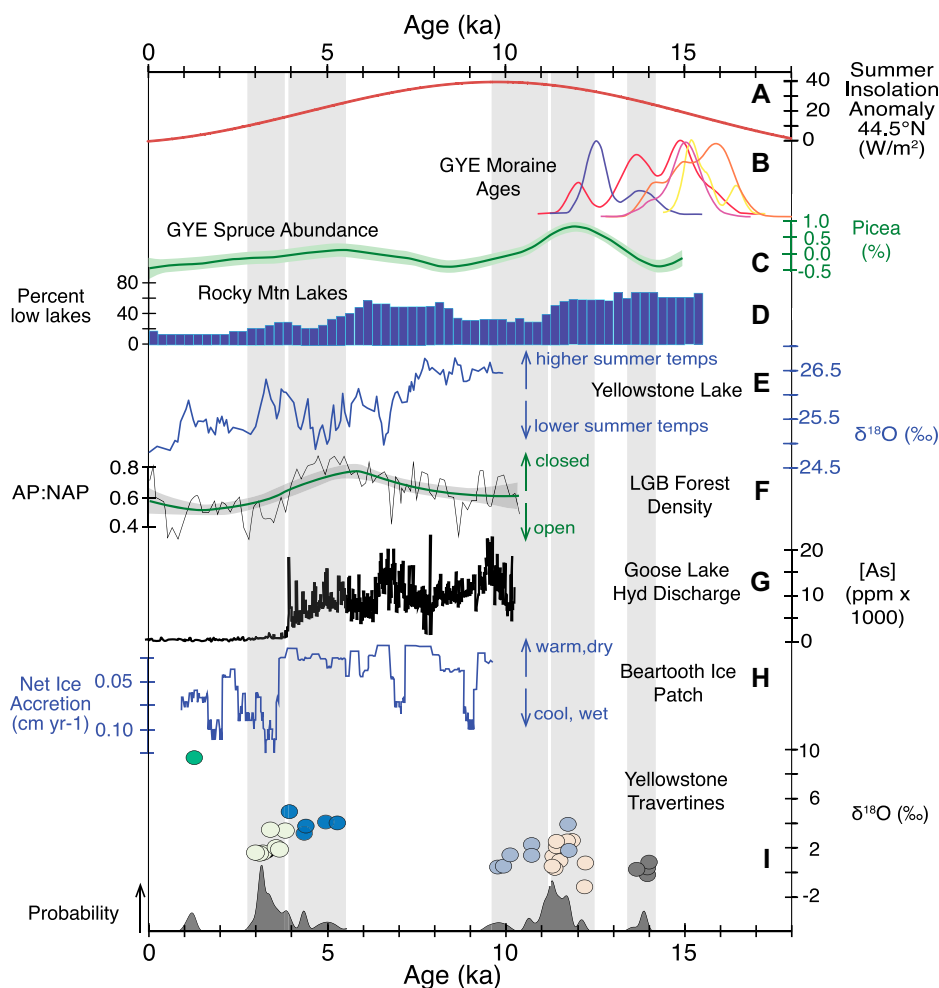


**Figure 7.** (A) Summer insolation anomaly (in  $\text{W/m}^2$ ) at  $44.5^\circ\text{N}$  (Berger, 1978). (B) Cosmogenic exposure probability density functions of moraine ages in the Yellowstone region (Licciardi and Pierce, 2018): purple curve—Lake Solitude, Teton County, Wyoming; red curve—Inner Jenny Lake, Teton County, Wyoming; yellow curve—Pinedale 2, Teton County, Wyoming; orange curve—Outer Jenny Lake, Teton County, Wyoming; magenta curve—Junction Butte, northern Yellowstone National Park. GYE—Greater Yellowstone Ecosystem. (C) Modeled composite *Picea* abundance in the Yellowstone region (*Picea engelmannii* was among the first conifers to colonize the deglaciated landscape, as it is frost tolerant and can endure long, cold winters and short, cool summers; Krause and Whitlock, 2017). (D) Composite lake-level history based on percent of lakes located within the U.S. Rocky Mountains that were  $>0.5$  standard deviations below their mean level per 250 yr interval (Shuman and Serravezza, 2017). (E) Yellowstone Lake  $\delta^{18}\text{O}_{\text{diatom}}$  measured in fossil diatoms from lake sediment cores (Brown et al., 2021). (F) Goose Lake ratio of arboreal pollen to nonarboreal pollen (AP:NAP), an indication of the local forest density (Schiller et al., 2022). LGB—Lower Geyser Basin. (G) Goose Lake hydrothermal history based on arsenic concentration in sediment cores; higher arsenic concentrations indicate a higher input of hydrothermal water (Schiller et al., 2022). (H) Beartooth ice patch net ice-accretion rate (in  $\text{cm yr}^{-1}$ ), where lower ice accretion indicates warmer temperatures and less winter precipitation (Chellman et al., 2021). (I) Travertine  $\delta^{18}\text{O}_{\text{carbonate}}$  and age probability density curve from this study plotted with regional and local paleoclimate indicators. Vertical gray bands indicate time periods of Yellowstone intracaldera travertine deposition.

This regime lasted as long as the large volumes of cold, meteoric water increased surficial weathering and supplied recharge with higher

total dissolved solids (Fig. 2A). As the glaciers disappeared and surficial conditions dried, cold meteoric water infiltration decreased, and ther-

mal waters became less reactive with subsurface rhyolite due to the higher temperatures of water-rock interaction. Higher thermal water temperatures also resulted in more boiling and calcite precipitation in the deeper subsurface, further decreasing concentrations of calcium and bicarbonate ions in thermal waters discharging at the surface. Consequently,  $\text{Ca}^{2+}$  and total alkalinity concentrations would have declined to a point where calcite saturation could not be maintained, similar to modern hydrothermal conditions within the Yellowstone caldera, where travertine deposition does not occur.

Although the scenario of intracaldera travertine deposition illustrated above uses the high melt-water volumes produced during glacial recession as the source of cold water to the hydrothermal system, the same processes would operate if extended periods of high precipitation caused substantial increases in meteoric water recharge to the Yellowstone hydrothermal system. This concept is supported by data from frequent sampling of rivers that drain thermal areas in the Yellowstone caldera. The ratios of  $\text{HCO}_3^-/\text{Cl}^-$  and  $\text{Ca}^{2+}/\text{Cl}^-$  and the total discharge of  $\text{HCO}_3^-$  and  $\text{Ca}^{2+}$  increase substantially during elevated fluvial discharge following annual snowmelt (Hurwitz et al., 2010). This observation suggests that more meteoric water recharge into the subsurface increases the concentrations of  $\text{HCO}_3^-$  and  $\text{Ca}^{2+}$  in groundwater, which, when scaled to higher precipitation levels than observed during historical monitoring, may significantly increase the propensity for travertine deposition.

Finally, evidence for the calcite buffering capacity of the subsurface hydrothermal system is illustrated by the oxygen isotope composition of hydrothermal minerals analyzed from several research cores drilled in the Upper and Lower Geyser Basins in the late 1960s (White et al., 1975). The stable isotope composition of hydrothermal quartz and clay minerals at depth was not in equilibrium with the  $\delta^{18}\text{O}$  of present-day thermal waters, whereas that of calcite was in equilibrium (Sturchio et al., 1990). This discrepancy suggests that quartz and clays are unreactive over time and with chemical changes in the hydrothermal system, whereas calcite is continuously dissolved and precipitated with changing hydrothermal conditions, cycling with the amount of  $\text{CO}_2$  and  $\text{Ca}^{2+}$  supplied and temperature of the reservoir.

### Travertine Stable Isotope and Geochemical Signals

#### Travertine Elemental Compositions: Higher Rates of Surficial Weathering in the Past

The Pinedale glaciation spanned from ca. 22 ka to 14.5 ka on the Yellowstone Plateau, based on



cosmogenic nuclide exposure dating of ice-marginal features and radiocarbon dating of postglacial lake sediments (Licciardi and Pierce, 2018; Whitlock, 1993). Subaerial travertine deposition was initiated at Hillside Springs at ca.  $13.9 \pm 0.12$  ka, providing a minimum age for glacial recession in the Upper Geyser Basin. The elevated CIA with low Ca/(Mg + Ca) and  $\delta^{18}\text{O}$  values of Old Hillside Springs travertines suggest deposition from waters that contained a significant component of surficial glacial meltwater (Fig. 6).

The low Ca/(Mg + Ca) ratio in postglacial travertines was a result of the weathering of exotic glacially transported sediment (Fig. 6A). Because high-silica rhyolites underlying the Yellowstone caldera are Ca- and Mg-poor rocks, sediments with higher calcium and magnesium are required to explain the elevated magnesium concentrations in the oldest Hillside travertines. A likely source for these sediments would have been the basaltic and andesitic Absaroka volcanics located in the northeastern sector of the Yellowstone region, transported west by glaciers that originated northeast or east of Yellowstone National Park in the Beartooth uplift or volcanic Absaroka Range (Licciardi and Pierce, 2018). Substantial deposits of Pinedale-age till and glacial kame in the Upper and Lower Geyser Basins confirm the occurrence of locally high sedimentation rates in postglacial time, as does carbonate-bearing Pinedale-age loess deposits in Jackson Hole, Wyoming (Waldrop, 1975; Waldrop and Pierce, 1975; Muffler et al., 1982a, 1982b; Pierce et al., 2011). Significantly, Pinedale-age loess exhibits significant calcium and magnesium leaching in the top 2 m, indicating that snowmelt and precipitation in postglacial times were high enough to extensively leach labile elements from fresh reactive deposits (Pierce et al., 2011). Similarly high rates of sedimentation from glacial outwash are also recorded in Blacktail and Slough Creek ponds in northern Yellowstone National Park (Krause and Whitlock, 2013; Whitlock et al., 2012).

#### **Travertine Stable Isotopes: Variations in Paleowater Composition**

The  $\delta^{18}\text{O}$  values of paleowaters that deposited travertine were likely 2‰–4‰ lower than present-day surficial waters within the Upper Geyser Basin (approximately  $-18.2\text{‰}$  at Hillside Springs; McCleskey et al., 2022), indicating either a glacial meltwater source ( $-23\text{‰}$  to  $-25\text{‰}$  for Pleistocene ice; Bindeman and Lowenstern, 2016) or cold late-glacial precipitation (2‰–4‰ lower than present-day precipitation based on isotope measurements of fossilized teeth in the western United States; Kohn and McKay, 2010).

To assess the stable isotope compositions of travertines, we calculated the theoretical  $\delta^{18}\text{O}$  that would be in equilibrium with present-day thermal waters at Hillside Springs ( $\delta^{18}\text{O}_{\text{water}} \approx -18.2\text{‰}$ ; McCleskey et al., 2022) using the fractionation factor–temperature equation of Kele et al. (2015), which was calibrated for temperatures up to 90 °C. The maximum temperature a travertine can precipitate subaerially is 92 °C, which is the boiling temperature of pure water at the local elevation. Travertine formed from water with  $\delta^{18}\text{O}_{\text{water}} = -18.2\text{‰}$  at this temperature has an equilibrium  $\delta^{18}\text{O}_{\text{carbonate}}$  of 0.40‰. This value is too high to account for the lowest  $\delta^{18}\text{O}_{\text{carbonate}}$  values of the late Pleistocene travertines from Hillside Springs and some of the oldest travertines near Morning Glory Pool (Fig. 4C). Furthermore, travertines typically precipitate from waters that are 10–30 °C cooler than the boiling temperature, further increasing the value of equilibrium travertine  $\delta^{18}\text{O}_{\text{carbonate}}$ . Other processes in this system, including reactions between meteoric waters and subsurface rhyolite ( $\delta^{18}\text{O}_{\text{rhyolite}} \approx 6\text{‰}$ ; Bindeman and Lowenstern, 2016) and steam separation at depth, will further increase the thermal water  $\delta^{18}\text{O}_{\text{water}}$  to more positive values (McKenzie and Truesdell, 1977). Therefore, it is impossible to explain the  $\delta^{18}\text{O}_{\text{carbonate}}$  of the oldest travertines without requiring much lower  $\delta^{18}\text{O}_{\text{water}}$  in the recharge water, to allow values down to  $-22\text{‰}$  in discharging paleowaters. To illustrate, the calculated  $\delta^{18}\text{O}_{\text{water}}$  of paleowaters in equilibrium with measured  $\delta^{18}\text{O}_{\text{carbonate}}$  values at a reasonable temperature range of 70–80 °C requires  $\delta^{18}\text{O}_{\text{water}}$  values between  $-19.5\text{‰}$  and  $-22.2\text{‰}$  for Old Hillside (Fig. 4C). If these calculated  $\delta^{18}\text{O}_{\text{water}}$  values are plotted on the global meteoric water line with modern Yellowstone cold surface waters, the paleowaters that formed travertines at Old Hillside, some of those at Hillside Springs, and those near Morning Glory Pool were lower in  $\delta^2\text{H}$  and  $\delta^{18}\text{O}$  values than any known modern precipitation source (Rye and Truesdell, 2007; Fig. 4D). For comparison, all modern Mammoth Hot Spring travertines have a  $\delta^{18}\text{O}_{\text{carbonate}} = 1.88\text{‰}$ – $9.61\text{‰}$ , which were deposited from 28 °C to 73 °C waters that have  $\delta^{18}\text{O}_{\text{water}}$  values between  $-16.6\text{‰}$  and  $-18.3\text{‰}$ . These modern calcite values are comparable to those measured in younger travertines from North Hillside, Firehole Lake, and Terrace Spring (Fig. 4A; Friedman, 1970; Chafetz and Lawrence, 1994; Fouke et al., 2000).

The  $\delta^{13}\text{C}_{\text{carbonate}}$  values vary between  $-0.70\text{‰}$  at North Hillside travertines to 4.23‰ in Morning Glory Pool travertines, with no consistent trend with time (Fig. 4). The Yellowstone ecosystem is dominated by C3-type vegetation

and has been since deglaciation, resulting in no drastic variations in  $\delta^{13}\text{C}$  from the transition from late-glacial tundra to present-day forest. Consistent travertine  $\delta^{13}\text{C}$  values through time and between the different intracaldera travertine deposits indicate that the source of carbon to thermal waters was dominated by deep sources of carbon, not shallow ones, which likely would have varied isotopically with differences in climate, soil respiration, and vegetation. Most (78%) modern diffuse soil  $\text{CO}_2$   $\delta^{13}\text{C}$  values are in the range of Yellowstone fumarole gases, which are slightly lower than the  $\delta^{13}\text{C}$  values of most intracaldera travertine (Moran et al., 2017; Werner and Brantley, 2003; Rahilly and Fischer, 2021). These data are evidence that a major source of  $\text{CO}_2$  in thermal waters is magmatic gas from the deep, long-lived Yellowstone magmatic reservoir, which produces a dispersed and relatively constant flux across the Yellowstone Plateau Volcanic Field (Fig. 4; Moran et al., 2017; Werner and Brantley, 2003; Rahilly and Fischer, 2021). It is impossible to resolve with stable carbon and oxygen isotopes whether the  $\delta^{13}\text{C}_{\text{carbonate}}$  of intracaldera travertines is a result of (1) mixing between this deep magmatic gas ( $\delta^{13}\text{C} = -3\text{‰}$ ;  $\delta^{18}\text{O} = -21\text{‰}$ ) and sedimentary rocks in the subsurface (average  $\delta^{13}\text{C} = 0.6\text{‰}$ ;  $\delta^{18}\text{O} = 20\text{‰}$ ) followed by kinetic fractionation of carbon isotopes driven by rapid subaerial  $\text{CO}_2$  degassing or (2) boiling of subsurface fluids followed by kinetic fractionation with subaerial  $\text{CO}_2$  degassing (Fig. 4B). We find it likely that the first scenario is more probable given that any significant subsurface boiling would have precipitated calcium carbonate underground and therefore may not have resulted in surficial travertine deposits. It should be noted that Mammoth Hot Spring travertines have higher  $\delta^{18}\text{O}_{\text{carbonate}}$  and  $\delta^{13}\text{C}_{\text{carbonate}}$  values that trend toward the composition of Madison Limestone rocks of Mississippian age (Fig. 4B; Pierce et al., 1991; Kharaka et al., 1991) and therefore Mississippian-age seawater values, providing an indication of greater sedimentary input north of the caldera than within the caldera (Fig. 4B). The transition from the vent to pond to distal facies of Mammoth Hot Springs travertine shows 2.3‰ variation in  $\delta^{13}\text{C}$  and 4.6‰ variation in  $\delta^{18}\text{O}$  over 6 m because of degassing of isotopically light  $\text{CO}_2$  along the flow path (Fouke et al., 2000); this observation is consistent with rapid kinetic isotopic fractionation and surficial  $\text{CO}_2$  degassing (vertical trend in Fig. 4B).

#### **Travertine Strontium Isotopes: An Indication of Subsurface Water Flow Path**

Thermal water plumbing paths of paleowaters for each travertine deposit are inferred from the

$^{87}\text{Sr}/^{86}\text{Sr}$  isotopic ratios of the travertines (Fig. 5). Water-rock reactions and carbonate precipitation are understood to not cause strontium isotopic fractionation, so the isotopic composition of discharging thermal waters and travertines is a record of the strontium isotopic composition of the rock, or at least the most leachable fraction of the rock, with which the water equilibrated. The uniform Sr isotopic composition for each group of travertines from different locations supports this assumption and indicates that the plumbing path for each travertine thermal system was unique.

The pathway of groundwater discharge that produced the travertine near Morning Glory Pool was very different from present-day thermal waters in the Upper Geyser Basin, based on the much higher  $^{87}\text{Sr}/^{86}\text{Sr}$  value of present-day thermal waters as compared to the travertines near Morning Glory Pool. Instead of being fed by the main thermal fluid flowing upward in the Upper Geyser Basin, which likely equilibrated with the underlying Biscuit Basin rhyolite flows (Fig. 5A), thermal waters responsible for the travertine near Morning Glory Pool likely equilibrated with the Lava Creek Tuff (Fig. 5B), known to be cryptically and heterogeneously present in the shallow subsurface in uplifted fault blocks (Keith and Muffler, 1978), rather than the nearby Mallard Lake flow with lower  $^{87}\text{Sr}/^{86}\text{Sr}$ . Terrace Spring  $^{87}\text{Sr}/^{86}\text{Sr}$  isotope ratios are also consistent with a flow path through the Lava Creek Tuff, which is unsurprising given that this spring discharges from the base of a cliff of Lava Creek Tuff on the caldera ring fault (Waldrop and Pierce, 1975). The other travertines are similar in strontium isotopic composition to rhyolite flows of the Central Plateau Member of the Plateau Formation or the Mallard Lake flow of the Upper Basin Member of the Plateau Formation, indicating flow paths through these units, likely in the highly permeable autobrecciated contact zones between flows (Finn et al., 2022). Equilibration of thermal fluids with the more reactive glass may have resulted in thermal water  $^{87}\text{Sr}/^{86}\text{Sr}$  isotopic ratios that were slightly lower than the whole rock because the glasses of some rhyolite flows are slightly more primitive than their crystal cargo from the injection of more mafic magma shortly prior to eruption (Loewen et al., 2017).

### Travertine Deposition Timing: Climatic and Tectonic Connections

#### *Late Pleistocene (14.5–10 ka): Deglaciation and the Younger Dryas*

The initial postglacial deposition of travertine at Hillside Springs occurred from 13.9 ka to 13.5 ka and closely postdated cosmogenic

exposure ages of late Pinedale glaciation recessional moraines located both north and south of the geyser basins (Fig. 7B; Licciardi and Pierce, 2018). Because ice recession likely occurred from west to east over the Upper and Lower Geyser Basins, the lack of travertine dating to 13.9–13.5 ka on the eastern side of the basins may indicate that they were still covered by ice, that there was active glacial outwash at this time that prevented or buried travertine deposits, or that deposits of this age are no longer exposed. At Hillside Springs, travertine deposition ceased after ~500 years, suggesting that the effects of glacial meltwater infiltration were short-lived, or surficial conditions prevented travertine deposition and/or preservation between 13.5 ka and 12.2 ka.

Based on the current sampling resolution, more voluminous deposition of travertine commenced at  $12.2 \pm 0.2$  ka at Hillside Springs, representing an episode that appears to have commenced 700 years into the Younger Dryas cold event (ca. 12.9–11.7 ka; Cheng et al., 2020) and continued until 9.5 ka (Fig. 3). Travertine ages do not align with the beginning of the Younger Dryas, which suggests that: (1) the Yellowstone hydrothermal system response lagged behind a climate trigger by hundreds of years, (2) cooling was not strongly registered in this region before 12.2 ka, or (3) the early part of the Younger Dryas was cool but not sufficiently wet. It is also possible that the Yellowstone hydrothermal system has a significant buffering capacity (via the precipitation and dissolution of subsurface calcite) and requires sustained high inputs of meteoric water to impact thermal water chemistry. All travertine deposits investigated here are located near the edges of geyser basins. Their location suggests that chemical transformations of discharging groundwater were confined to the edges of geyser basins, where mixing between cool meteoric water-fed aquifers and upwelling basin thermal waters was greatest (e.g., Finn et al., 2022) and where the maximum temperatures of recharge waters heated in the subsurface would be lowest.

The climate and environment of the Yellowstone region during the Younger Dryas cold period are poorly known. Some, but not all, cirque glaciers in the Wind River Mountains (Gosse et al., 1995; Dahms et al., 2018), Beartooth Mountains (Barth et al., 2022), and across the western United States (Marcott et al., 2019) experienced readvances or standstills during this time. A standstill moraine at Emerald Lake in the Beartooth uplift, for example, has a low aspect ratio, suggesting a short-lived, minor climate excursion or period of low sediment deposition during a pause in glacial retreat (Barth et al., 2022). Similarly, the youngest exposure

age for moraines in the Tetons is attributed to a minor glacial standstill during early Younger Dryas time (Lake Solitude, Fig. 7B; Licciardi and Pierce, 2018). In most cases, regional glaciers did not experience significant advances during Younger Dryas time.

Younger Dryas cooling is also not clearly recorded in pollen records from the Yellowstone region, possibly because: (1) the pollen sampling interval lacks the resolution to capture a short-lived event, (2) the region did not experience significant climate change, or (3) the subalpine mixed-conifer forest at the time was relatively insensitive to cool conditions (Whitlock et al., 2008, 2012; Krause and Whitlock, 2013). Blacktail Pond, located in northern Yellowstone National Park, shows low  $\delta^{18}\text{O}$  values in authigenic carbonates that indicate less lake-water evaporation along with pollen indicative of treeless vegetation during the Younger Dryas (Krause and Whitlock, 2013).

The initial deglacial landscape of the central Yellowstone Plateau was choked with till, outwash, and loess. As the climate warmed after 13 ka, different conifers started to move into the Yellowstone region and become established. One of the early species, Engelmann spruce (*Picea engelmannii*), colonized between 13 ka and 11.5 ka at all elevations and apparently at the same time as formation of travertine at Hillside Springs and near Morning Glory (Fig. 7C; Krause and Whitlock, 2017). Soil development and related weathering of sediments were likely important factors for both early forest establishment and travertine formation, reflecting a lag of centuries between deglaciation and sufficient weathering to establish soils and increase the total dissolved solids in infiltrating meteoric waters.

#### *Early to Mid-Holocene (11–5 ka)*

Travertine deposition continued until 11.1 ka at Hillside Springs and from ca. 11.7 ka to 9.5 ka near Morning Glory Pool before hydrothermal systems transitioned back to silica sinter deposition because of the warmer, drier summer conditions of the early to middle Holocene (Whitlock, 1993; Larsen et al., 2020; Chellman et al., 2021; Schiller et al., 2022). These climatic changes are attributed to the amplification of the seasonal cycle of insolation (Fig. 7A; Bartlein et al., 1998). Travertine deposition seems to have ceased concurrently with climatic drying at Hillside Springs (at 11.1 ka), whereas travertine deposition near Morning Glory Pool did not stop until ca. 9.5 ka, possibly because its thermal waters were supported by a larger source of calcium and magnesium from recharge through thicker deposits of Pinedale till on the east side of Upper Geyser Basin than the west. It is also

noteworthy that Minnetonka Cave, located in the Wasatch Mountains in southeastern Idaho, also ceased depositing speleothem calcite at ca. 9.5 ka (Lundeen et al., 2013), coincident with cessation of travertine deposition near Morning Glory Pool.

Strong support for warm, dry conditions near the geyser basins comes from  $\delta^{18}\text{O}$  data determined from fossil diatoms preserved in Yellowstone Lake cores, which indicate high lake-water evaporation from 9.9 ka (the beginning of the record) to 7.5 ka (Fig. 7E; Brown et al., 2021). Pollen records from the central and southern Yellowstone region show an expansion of lodgepole pine (*Pinus contorta*) and notable increases in Douglas fir (*Pseudotsuga menziesii*) and aspen (*Populus tremuloides*) between 10 ka and 5 ka, and a charcoal record from the central Yellowstone region indicates higher fire activity in the early and middle Holocene than at present (Whitlock, 1993). Lake levels were also lower than present from 11.3 ka to 5.7 ka and especially from 9.3 ka to 5.7 ka in the Yellowstone region and throughout the Rocky Mountains (Fig. 7D; Shuman and Serravezza, 2017; Whitlock et al., 2012; Krause and Whitlock, 2013).

#### Late Holocene (5 ka–Present)

After ca. 6 ka, decreased summer insolation resulted in cooler, wetter conditions than before, leading to an ecological transformation from open forest to closed forest and from small frequent to large infrequent fires in the central Yellowstone region (Fig. 7F; Whitlock, 1993; Schiller et al., 2022). Several paleoclimate proxies indicate cooler and wetter conditions during this interval than before ca. 6 ka. The  $\delta^{18}\text{O}$  data from Yellowstone Lake fossil diatoms register several cool events from 5.5 ka to 4.5 ka (Fig. 7E; Brown et al., 2021). Other indications of wet conditions starting around 5 ka include cessation of the Minnetonka Cave speleothem, increased rates of travertine deposition in the Salt Lake graben, increases in  $\delta^{18}\text{O}$  values recorded from the Beartooth ice patch, which indicate warmer winter temperature and greater snowpack than before, and the rise of Rocky Mountain lake levels, which is consistent with more snowpack and/or less evaporation (Lundeen et al., 2013; Kampman et al., 2012; Shuman and Marsicek, 2016; Chellman et al., 2021; Fig. 7). Deposition of travertine at North Hillside started at  $5.2 \pm 0.04$  ka and lasted  $\sim 1340$  years, coinciding with this wetter regional climate.

Firehole Lake travertine deposition occurred between 3.8 ka and 3.0 ka, and its onset may have been caused by hydrothermal system reorganization or a continuation of late Holocene wet conditions. It is also important to note that the exposed Firehole Lake travertine may only be the top of a

thicker deposit, as is suggested by the presence of travertine between 8 m and 10 m depth in the Y-2 research drill core located less than 50 m west of the sampled surficial deposit (Fig. 1B; Bargar and Beeson, 1981). Regardless of the presence of older travertines, ca. 3.8 ka coincides with cessation of deposition of the Minnetonka Cave speleothem due to cool, wet conditions, greatly increased ice accretion in the Beartooth ice patch due to cooler conditions with continued high precipitation, a modest decrease in lake levels in the region, and the highest deposition rates in the Salt Lake graben record (Lundeen et al., 2013; Kampman et al., 2012; Shuman and Marsicek, 2016; Chellman et al., 2021; Fig. 7).

Geochemical, pollen, and diatom records from nearby Goose Lake in Lower Geyser Basin (Schiller et al., 2022) show a sharp decline in arsenic concentrations and cooler water conditions at 3.8 ka, which are interpreted as evidence of thermal water ceasing to flow into Goose Lake. This shift in hydrothermal activity coincided with the opening of the forest and less fire activity in the Lower Geyser Basin and the deposition of Firehole Lake travertine (Fig. 7G; Schiller et al., 2022). The coincidence of travertine deposition at Firehole Lake with hydrothermal changes at Goose Lake suggests a possible seismic event that reorganized the hydrothermal plumbing system of the Lower Geyser Basin, which could have released a pulse of accumulated  $\text{CO}_2$  (Uysal et al., 2009). Alternatively, the unexposed Firehole Lake travertines may have started forming earlier in time, perhaps dating to the earlier North Hillside event at 5.2 ka and cool conditions.

After ca. 3.0 ka, lower  $\delta^{18}\text{O}_{\text{diatom}}$  values from Yellowstone Lake indicate less evaporative effect, implying cooler summers and coinciding with the end of Firehole Lake travertine deposition at  $3.0 \pm 0.07$  ka (Fig. 7E; Brown et al., 2021). A period of neoglaciation advances started in the Teton Mountains at 4 ka and ended at ca. 2.5 ka, after which increases in sedimentation rate indicate lower precipitation conditions (Larsen et al., 2020). Concurrently, a decrease in net ice-accretion rate in the Beartooth ice patch after 2 ka indicates warming, as does the increase in ice-patch  $\delta^{18}\text{O}_{\text{ice}}$  values; increases in  $\delta^{18}\text{O}_{\text{carbonate}}$  at Crevice Lake were likely related to less snowpack; and decreases in Salt Lake graben travertine deposition rates imply warming conditions (Chellman et al., 2021; Whitlock et al., 2012; Kampman et al., 2012; Fig. 7).

Values of  $\delta^{18}\text{O}$  in the Yellowstone Lake diatom record were slightly higher from ca. 2 ka to 1 ka, indicating periods of more lake-water evaporation during the Roman Warm Period (2.2–1.55 ka) and Medieval Climate Anomaly (1.2–0.7 ka; Brown et al., 2021). This period

also includes deposition of the Terrace Spring travertine, which is a thinly exposed veneer constrained to  $1.26\text{--}1.06 \pm 0.01$  ka. This period was associated with drought and widespread aridity in western North America, representing unlikely conditions for travertine formation. However, the deposit is roughly coincident with a large earthquake on the  $\sim 25$ -km-long Eagle Bay fault zone in Yellowstone Lake, where displacements of 1 m are evident in lake bottom sediments. The age of this large earthquake is inferred to be ca. 1.5 ka (Morgan et al., 2023), and substantial shaking on the Yellowstone Plateau could have fractured a pathway for trapped  $\text{CO}_2$  gas to escape to the surface, especially in preexisting fault zones. Springs with mantle-derived helium isotopic compositions are typically associated with deep faults that serve as conduits for high  $\text{CO}_2$  fluxes and may assist with saturating thermal waters with calcite at the surface (e.g., Uysal et al., 2009). Terrace Spring has among the highest helium isotope compositions observed in Yellowstone National Park ( $R_c/R_a \approx 7.9$ ; Lowenstern et al., 2005) along with exceptionally high  $\text{CO}_2$  concentrations. Furthermore, Terrace Spring is located at the intersection of the caldera rim and major north-south-trending faults (Bergfeld et al., 2014). These major structural features likely act as high-permeability pathways for fluids and volatiles when major seismic events rupture hydrothermally sealed systems (Uysal et al., 2009).

The Terrace Spring deposit is interpreted to have precipitated as a result of a short-lived, seismically induced release of  $\text{CO}_2$  that led to travertine deposition without substantial changes to thermal water chemistry, as indicated by the fact that the  $^{87}\text{Sr}/^{86}\text{Sr}$  isotopic ratio of the travertine is in equilibrium with modern-day Terrace Spring waters (Fig. 6). The absence of other intracaldera travertine deposits at this time suggests that thermal waters in most areas of the Upper and Lower Geyser Basins did not have enough available calcium for travertine formation, regardless of any seismically induced pulses of  $\text{CO}_2$  release. Although intracaldera travertine deposition may have been supported by  $\text{CO}_2$  leakage from seismic activity in the past (e.g., Terrace Spring), the main driving force behind travertine deposition was likely the influx of large volumes of cold meteoric water that decreased the temperature of water-rock reactions and increased the rate of chemical weathering of surficial sediments, as shown by the correspondence between the timing of travertine deposition and wet climatic conditions.

#### Travertine Deposit Volume and $\text{CO}_2$ Flux

The pulsed timing of intracaldera hydrothermal travertine deposition that corresponds with

TABLE 1. CO<sub>2</sub> FLUX CALCULATED FROM YELLOWSTONE NATIONAL PARK INTRACALDERA TRAVERTINE VOLUME

| Location           | Surface area of travertine outcrop (m <sup>2</sup> ) | Estimated thickness of deposit (m) | Minimum age (ka) | Maximum age (ka) | Volume (m <sup>3</sup> ) | CO <sub>2</sub> * (metric tons) | CO <sub>2</sub> flux (tons/yr) | CO <sub>2</sub> flux (tons/d) |
|--------------------|--|------------------------------------|------------------|------------------|--------------------------|---------------------------------|--------------------------------|-------------------------------|
| Hillside Springs   | 138,797  | 4                                  | 11.1             | 13.9             | 5.5 × 10 <sup>5</sup>    | 5.8 × 10 <sup>5</sup>           | 2.1 × 10 <sup>2</sup>          | 0.6                           |
| N. Hillside Spring | 310  | 3                                  | 3.9              | 5.2              | 7.8 × 10 <sup>2</sup>    | 8.0 × 10 <sup>2</sup>           | 1                              | 0.0                           |
| Morning Glory      | 1973   | 1                                  | 9.5              | 11.7             | 1.9 × 10 <sup>3</sup>    | 2.0 × 10 <sup>3</sup>           | 1                              | 0.0                           |
| Firehole Lake      | 24,710   | 3                                  | 3.0              | 3.8              | 7.5 × 10 <sup>3</sup>    | 7.8 × 10 <sup>3</sup>           | 10                             | 0.0                           |
| Terrace Spring     | 298,110  | 1                                  | 1.1              | 1.2              | 1.5 × 10 <sup>5</sup>    | 1.5 × 10 <sup>5</sup>           | 1.5 × 10 <sup>3</sup>          | 4.2 <sup>†</sup>              |
| TOTAL              | 463,900  | 11                                 | —                | —                | 7.1 × 10 <sup>5</sup>    | 7.4 × 10 <sup>5</sup>           | 1.8 × 10 <sup>3</sup>          | 5                             |

\*We assumed the density of calcite is 2.7 g/cm<sup>3</sup>, travertine porosity is 10%, and the mineralogy is 97% CaCO<sub>3</sub> for a bulk density of 2.43 g/cm<sup>3</sup>. The flux of CO<sub>2</sub> was calculated according to the equation  $\text{moles}_{\text{CO}_2} = \text{moles}_{\text{CaCO}_3} = (V \times \rho_b \times f_{\text{CaCO}_3})/M$ , where  $V$  is volume,  $\rho_b$  is the bulk density,  $f$  is the fraction of CaCO<sub>3</sub> in travertine, and  $M$  is the molar mass of CaCO<sub>3</sub> (Mancini et al., 2019).

<sup>†</sup>The age of this deposit is not well constrained, and this value therefore has a high level of uncertainty. If the deposit formed over a greater time span, then the calculated flux would be smaller.

wet climate indicates that the flux of CO<sub>2</sub> within the Yellowstone caldera was relatively constant in postglacial time and that there was not a large, ephemeral release of CO<sub>2</sub> associated with deglaciation. Furthermore, the small volume of the travertine deposits within the caldera implies a limited spatial and temporal CO<sub>2</sub> flux (Table 1). To examine if an episodic large release of CO<sub>2</sub> could have triggered travertine deposition, we first calculated the total volume of intracaldera travertine deposits. Assuming a travertine bulk density of 2.43 g/cm<sup>3</sup> and a rough travertine volume based on mapped exposures and estimated thickness, the total amount of travertine in the Upper and Lower Geyser Basins is 0.0007 km<sup>3</sup>. This amount, when converted from calcite into CO<sub>2</sub> according to Equation 1 and following the method of Mancini et al. (2019), converts to ~740 metric kilotons CO<sub>2</sub>, equivalent to only approximately 1 month's worth of CO<sub>2</sub> derived from depth at the total current diffuse emission rate for all of the Yellowstone Plateau Volcanic Field (24 ± 12 kilotons CO<sub>2</sub> per day; Rahilly and Fischer, 2021). Inasmuch as the amount of CO<sub>2</sub> represented by the volume of travertine deposits studied here is spread out over time and space, the amount is even more negligible compared with the present-day flux.

Although it could be a result of preservation bias, the apparently smaller volume of North Hillside and Firehole Lake travertines suggests that late Holocene wet periods were either less extreme and shorter than earlier episodes and/or that the supply of fresh reactive sediments was much less than that available in the millennia following deglaciation. Regional climate proxies, especially Yellowstone Lake  $\delta^{18}\text{O}_{\text{diatom}}$ , indicate that regional climate from ca. 6 ka to 4 ka was highly variable with more frequent, short-duration fluctuations between wet and dry conditions (Fig. 7E; Brown et al., 2021). This provides evidence that smaller late Holocene travertine deposits may indeed have been a result of shorter and less extreme climate events.

The absence of appreciable subsurface travertine deposits in research drill cores from the

Upper and Lower Geyser Basins suggests that large, buried travertine deposits on the scale observed at Mammoth Hot Springs do not exist underneath the present-day silica-sinter deposits. Hydrothermal travertine may have been deposited during or prior to the last glaciation and during major magmatic shallow intrusions or eruptions; however, any evidence of such deposits has been obliterated by recent large rhyolite flows (at 162 ka, 111 ka, and 70 ka; Christiansen, 2001; Stelten et al., 2023) and glaciations at ca. 160–130 ka and 22–14.5 ka (Licciardi and Pierce, 2018). Finally, within the Yellowstone caldera, the volume of travertine is not directly proportional to the flux of CO<sub>2</sub> for two reasons. First, a significant amount of CO<sub>2</sub> discharge is likely to occur through fumaroles and thermal features directly outgassing large amounts of CO<sub>2</sub> that have separated from deeper thermal fluids. Second, the occurrence and rate of travertine deposition are not 1 mol CaCO<sub>3</sub> deposited to 1 mol of CO<sub>2</sub> degassed because this system is not CO<sub>2</sub> limited; instead, it is typically limited by low calcium concentrations. Therefore, the calculated CO<sub>2</sub> fluxes based on volumes of intracaldera travertine are minimum estimates. Nevertheless, the very small volumes of postglacial-age travertine within the Yellowstone caldera do not suggest that there was a large postglacial surge in CO<sub>2</sub>.

## CONCLUSION

New <sup>230</sup>Th-U ages show that rare travertine deposits within the Yellowstone caldera formed during three episodes that correspond with known wet climate periods. Travertine deposition during wet climate was the result of increased amounts of meteoric water input into the shallow hydrothermal system, which decreased reservoir water temperatures and subsurface boiling while increasing the reactivity of thermal fluids with rock. These changes to the hydrothermal system were buffered by the dissolution and precipitation of calcite deep within the system, so calcium carbonate saturation

upon discharge only occurred where hydrothermal waters were coolest around the edges of main thermal basins and only for short periods (centuries to a few millennia). The small volume of these deposits, especially the vanishingly small amount of travertine with ages that closely postdate Pinedale glaciation, suggests no significant or sustained surge in CO<sub>2</sub> during the early postglacial period; instead, late Pleistocene and early Holocene travertine was primarily a result of an increased supply of calcium and magnesium associated with high rates of chemical weathering of fresh glacial deposits. Late Holocene travertine deposition was catalyzed by the same mechanism; that is, sustained periods of increased precipitation facilitated increased weathering and infiltration of labile elements, along with decreasing the temperature of water-rock interactions in the periphery of the hydrothermal system. The small volume of these deposits is consistent with the fact that late Holocene wet periods were less extreme and shorter than earlier episodes. Hydrothermal travertine deposited within the Yellowstone caldera is a unique indicator of paleoclimatic, seismic, and hydrochemical variations over geologic time and provides insight into the evolution of one of the largest and most dynamic hydrothermal systems in the world.

## ACKNOWLEDGMENTS

All samples were collected in cooperation with the National Park Service (NPS) under research permits YELL-2019-SCI-8030, YELL-2020-SCI-8158, and YELL-2021-SCI-8192; we thank the NPS for their assistance with the permitting and sampling process. We acknowledge support from the U.S. Geological Survey Mendenhall Program to L. Harrison, National Science Foundation grant 2149482 to C. Whitlock, and National Science Foundation grant 0125625 to J. Licciardi. We would like to thank Annie Carlson, Mara Reed, Dakota Churchill, Mark Stelten, and Behnaz Houssini for their assistance with permitting and sample collection. We are grateful to journal reviews from two anonymous reviewers; U.S. Geological Survey reviews by Greg Pederson, Michael Clynne, L.P. Muffler, and Kevin Jones; constructive comments from the associate editor, Alessandro Zanazzi; and efficient edi-



torial handling by Brad Singer. Any use of trade, firm, or product names is for descriptive purposes only and does not imply endorsement by the U.S. government.

## REFERENCES CITED

- Allen, E.T., and Day, A.L., 1935, The Hot Springs of the Yellowstone National Park: Carnegie Institute of Washington Publication 466, 525 p.
- Bargar, K.E., 1978, Geology and Thermal History of Mammoth Hot Springs, Yellowstone National Park, Wyoming: U.S. Geological Survey Bulletin 1444, 55 p., <https://doi.org/10.3133/b1444>.
- Bargar, K.E., and Beeson, M.H., 1981, Hydrothermal alteration in research drill hole Y-2, Lower Geyser Basin, Yellowstone National Park, Wyoming: The American Mineralogist, v. 66, p. 473–490.
- Bargar, K.E., and Fournier, R.O., 1988, Effects of glacial ice on subsurface temperatures of hydrothermal systems in Yellowstone National Park, Wyoming: Fluid-inclusion evidence: Geology, v. 16, p. 1077–1080, [https://doi.org/10.1130/0091-7613\(1988\)016<1077:EOGIOS>2.3.CO;2](https://doi.org/10.1130/0091-7613(1988)016<1077:EOGIOS>2.3.CO;2).
- Barth, A.M., Ceperley, E.G., Vavrus, C., Marcott, S.A., Shakun, J.D., and Caffee, M.W., 2022, <sup>10</sup>Be age control of glaciation in the Beartooth Mountains, USA, from the latest Pleistocene through the Holocene: Geochronology Discussions, v. 4, p. 731–743, <https://doi.org/10.5194/gchron-4-731-2022>.
- Bartlein, P.J., Anderson, P.M., Anderson, K.H., Edwards, M.E., Thompson, R.S., Webb, R.S., Webb, T., III, and Whitlock, C., 1998, Paleoclimate simulations for North America over the past 21,000 years: Features of simulated climate and comparisons with paleoenvironmental data: Quaternary Science Reviews, v. 17, p. 549–585, [https://doi.org/10.1016/S0277-3791\(98\)00012-2](https://doi.org/10.1016/S0277-3791(98)00012-2).
- Berger, A.L., 1978, Long-term variations of daily insolation and Quaternary climatic changes: Journal of the Atmospheric Sciences, v. 35, p. 2362–2367, [https://doi.org/10.1175/1520-0469\(1978\)035<2362:LTVODI>2.0.CO;2](https://doi.org/10.1175/1520-0469(1978)035<2362:LTVODI>2.0.CO;2).
- Bergfeld, D., Lowenstern, J.B., Hunt, A.G., Shanks, P., and Evans, W.C., 2014, Gas and Isotope Chemistry of Thermal Features in Yellowstone National Park, Wyoming: U.S. Geological Survey Scientific Investigations Report 2011-5012, 28 p., <https://pubs.usgs.gov/sir/2011/5012/>.
- Bergfeld, D., Lowenstern, J.B., Hunt, A.G., Hurwitz, S., McCleskey, B.R., and Peek, S.E., 2019, Chemical and Isotopic Data on Gases and Waters for Thermal and Non-Thermal Features across Yellowstone National Park (Ver. 2.0, March 2019): U.S. Geological Survey Data Release, <https://doi.org/10.5066/F7H13105>.
- Bindeman, I.N., and Lowenstern, J.B., 2016, Low δD hydration rinds in Yellowstone perlitites record rapid synruptive hydration during glacial and interglacial conditions: Contributions to Mineralogy & Petrology, v. 171, 89, <https://doi.org/10.1007/s00410-016-1293-1>.
- Bischoff, J.L., and Rosenbauer, R.L., 1996, The alteration of rhyolite in CO<sub>2</sub> charged water at 200 and 350°C: The unreactivity of CO<sub>2</sub> at higher temperature: Geochimica et Cosmochimica Acta, v. 60, no. 20, p. 3859–3867, [https://doi.org/10.1016/0016-7037\(96\)00208-6](https://doi.org/10.1016/0016-7037(96)00208-6).
- Brown, S.R., Cartier, R., Schiller, C.M., Zahajská, P., Fritz, S.C., Morgan, L.A., Whitlock, C., Conley, D.J., Lacey, J.H., Leng, M.J., and Shanks, W.C., 2021, Multi-proxy record of Holocene paleoenvironmental conditions from Yellowstone Lake, Wyoming, USA: Quaternary Science Reviews, v. 274, <https://doi.org/10.1016/j.quascirev.2021.107275>.
- Capezzuoli, E., Gandin, A., and Pedley, M., 2014, Decoding tufa and travertine (fresh water carbonates) in the sedimentary record: The state of the art: Sedimentology, v. 61, p. 1–21, <https://doi.org/10.1111/sed.12075>.
- Chafetz, H.S., and Guidry, S.A., 2003, Deposition and diagenesis of Mammoth Hot Springs Travertine, Yellowstone National Park, Wyoming, USA: Canadian Journal of Earth Sciences, v. 40, p. 1515–1529, <https://doi.org/10.1139/e03-051>.
- Chafetz, H.S., and Lawrence, J.R., 1994, Stable isotopic variability within modern travertines: Géographie Physique et Quaternaire, v. 48, p. 257–273, <https://doi.org/10.7202/033007ar>.
- Cheng, H., et al., 2020, Timing and structure of the Younger Dryas event and its underlying climate dynamics: Proceedings of the National Academy of Sciences of the United States of America, v. 117, no. 38, p. 23,408–23,417, <https://doi.org/10.1073/pnas.2007869117>.
- Chellman, N.J., Pederson, G.T., Lee, C.M., McWethy, D.B., Puseman, K., Stone, J.R., Brown, S.R., and McConnell, J.R., 2021, High elevation ice patch documents Holocene climate variability in the northern Rocky Mountains: Quaternary Science Advances, v. 3, <https://doi.org/10.1016/j.qsa.2020.100021>.
- Christiansen, R.L., 2001, The Quaternary and Pliocene Yellowstone Plateau Volcanic Field of Wyoming, Idaho, and Montana: U.S. Geological Survey Professional Paper 729-G, 145 p., <https://doi.org/10.3133/pp729G>.
- Coplen, T.B., 1994, Reporting of stable hydrogen, carbon, and oxygen isotopic abundances: Pure and Applied Chemistry, v. 66, p. 273–276, <https://doi.org/10.1351/pac199466020273>.
- Cullen, J.T., Hurwitz, S., Barnes, J.D., Lassiter, J.C., Penniston-Dorland, S., Kasemann, S.A., and Thordsen, J.J., 2019, Temperature-dependent variations in mineralogy, major element chemistry and the stable isotopes of boron, lithium, and chlorine resulting from hydration of rhyolite: Constraints from hydrothermal experiments at 150 to 350 °C and 25 MPa: Geochimica et Cosmochimica Acta, v. 261, p. 269–287, <https://doi.org/10.1016/j.gca.2019.07.012>.
- Dahms, D., Egli, M., Fabel, D., Harbor, J., Brandová, D., de Castro Portes, R., and Christl, M., 2018, Revised Quaternary glacial succession and post-LGB recession, southern Wind River Range, Wyoming, USA: Quaternary Science Reviews, v. 192, p. 167–184, <https://doi.org/10.1016/j.quascirev.2018.05.020>.
- De Boever, E., Jaramillo-Vogel, D., Bouvier, A.-S., Frank, N., Schröder-Ritzrau, A., Baumgartner, L., Swennen, R., and Foubert, A., 2022, The fate of a travertine record: Impact of early diagenesis on the Y-10 core (Mammoth Hot Springs, Yellowstone National Park, USA): The Depositional Record: A Journal of Biological, Physical and Geochemical Sedimentary Processes, v. 8, p. 220–250, <https://doi.org/10.1002/dep2.143>.
- Finn, C., Bedrosian, P.A., Holbrook, W.S., Auken, E., Bloss, B.R., and Crosbie, J., 2022, Geophysical imaging of the Yellowstone hydrothermal plumbing system: Nature, v. 603, p. 643–647, <https://doi.org/10.1038/s41586-021-04379-1>.
- Fouke, B.W., 2011, Hot-spring systems geobiology: Abiotic and biotic influences on travertine formation at Mammoth Hot Springs, Yellowstone National Park, USA: Sedimentology, v. 58, p. 170–219, <https://doi.org/10.1111/j.1365-3091.2010.01209.x>.
- Fouke, B.W., Farmer, J.D., Des Marais, D.J., Pratt, L., Sturchio, N.C., Burns, P.C., and Discipulo, M.K., 2000, Depositional facies and aqueous-solid geochemistry of the travertine-depositing hot springs (Angel Terrace, Mammoth Hot Springs, Yellowstone National Park, U.S.A.): Journal of Sedimentary Research, v. 70, no. 3, p. 565–585, <https://doi.org/10.1306/2DC40929-0E47-11D7-8643000102C1865D>.
- Fournier, R.O., 1989, Geochemistry and dynamics of the Yellowstone National Park hydrothermal system: Annual Review of Earth and Planetary Sciences, v. 17, p. 13–53, <https://doi.org/10.1146/annurev.ea.17.050189.000305>.
- Friedman, I., 1970, Some investigations of the deposition of travertine from hot springs—I. The isotopic chemistry of a travertine-depositing spring: Geochimica et Cosmochimica Acta, v. 34, p. 1303–1315, [https://doi.org/10.1016/0016-7037\(70\)90043-8](https://doi.org/10.1016/0016-7037(70)90043-8).
- Gosse, J.C., Evenson, E.B., Klein, J., Lawn, B., and Middleton, R., 1995, Precise cosmogenic <sup>10</sup>Be measurements in western North America: Support for a global Younger Dryas cooling event: Geology, v. 23, p. 877–880, [https://doi.org/10.1130/0091-7613\(1995\)023<0877:PCBBIW>2.3.CO;2](https://doi.org/10.1130/0091-7613(1995)023<0877:PCBBIW>2.3.CO;2).
- Harrison, L.N., Hurwitz, S., Paces, J.B., McCleskey, R.B., Roth, D.A., Conroy, R., and Stelten, M.E., 2022, Elemental and Strontium Isotopic Composition of Select Central Plateau and Upper Basin Member Rhyolites, Yellowstone Plateau Volcanic Field: U.S. Geological Survey Data Release, <https://doi.org/10.5066/P952ZE74>.
- Harrison, L.N., Hurwitz, S., Paces, J.B., and Peek, S., 2023, Radiogenic Sr Isotope Composition (<sup>87</sup>Sr/<sup>86</sup>Sr), Stable Oxygen and Carbon Isotope Composition, Elemental Concentrations, and U-Th Disequilibrium Ages for Travertine Deposits from Various Locations in Yellowstone National Park: U.S. Geological Survey Data Release, <https://doi.org/10.5066/P9G2R6ZF>.
- Hildreth, W., Halliday, A.N., and Christiansen, R.L., 1991, Isotopic and chemical evidence concerning the genesis and contamination of basaltic and rhyolitic magma beneath the Yellowstone Plateau volcanic field: Journal of Petrology, v. 32, no. 1, p. 63–138, <https://doi.org/10.1093/ptrology/32.1.63>.
- Hurwitz, S., and Lowenstern, J.B., 2014, Dynamics of the Yellowstone hydrothermal system: Reviews of Geophysics, v. 52, p. 375–411, <https://doi.org/10.1002/2014RG000452>.
- Hurwitz, S., Evans, W.C., and Lowenstern, J.B., 2010, River solute fluxes reflecting active hydrothermal chemical weathering of the Yellowstone Plateau Volcanic Field, USA: Chemical Geology, v. 276, no. 3–4, p. 331–343, <https://doi.org/10.1016/j.chemgeo.2010.07.001>.
- Kampman, N., Burnside, N.M., Shipton, Z.K., Chapman, H.J., Nicholl, J.A., Ellam, R.M., and Bickle, M.J., 2012, Pulses of carbon dioxide emissions from intracrustal faults following climatic warming: Nature Geoscience, v. 5, p. 352–358, <https://doi.org/10.1038/ngeo1451>.
- Keith, T.E.C., and Muffler, L.J.P., 1978, Minerals produced during cooling and hydrothermal alteration of ash flow tuff from Yellowstone drill hole Y-5: Journal of Volcanology and Geothermal Research, v. 3, p. 373–402, [https://doi.org/10.1016/0377-0273\(78\)90044-6](https://doi.org/10.1016/0377-0273(78)90044-6).
- Kele, S., Breitenbach, S.F.M., Capezzuoli, E., Meckler, A.N., Ziegler, M., Millan, I.M., Kluge, T., Deák, J., Hanselmann, K., John, C.M., Yan, H., Liu, Z., and Bernasconi, S.M., 2015, Temperature dependence of oxygen- and clumped isotope fractionation in carbonates: A study of travertines and tufas in the 6–95°C temperature range: Geochimica et Cosmochimica Acta, v. 168, p. 172–192, <https://doi.org/10.1016/j.gca.2015.06.032>.
- Kharaka, Y.K., Mariner, R.H., Bullen, T.D., Kennedy, B.M., and Sturchio, N.C., 1991, Geochemical investigations of hydraulic connections between Corwin Springs Known Geothermal Area and adjacent parts of Yellowstone National Park, in: Sorey, M., ed., Effects of Potential Geothermal Development in the Corwin Springs Known Geothermal Resources Area, Montana, on the Thermal Features of Yellowstone National Park: U.S. Geological Survey Water-Resources Investigations Report 91-4052, p. F1–F38, <https://doi.org/10.3133/wri914052>.
- Kharaka, Y.K., Thordsen, J.L., and White, L.D., 2002, Isotope and Chemical Compositions of Meteoric and Thermal Waters and Snow from the Greater Yellowstone National Park Region: U.S. Geological Survey Open-File Report 2002-194, 75 p., <https://doi.org/10.3133/ofr02194>.
- Kohn, M.J., and McKay, M., 2010, Stable isotopes of fossil teeth corroborate key general circulation model predictions for the Last Glacial Maximum in North America: Geophysical Research Letters, v. 37, L22702, <https://doi.org/10.1029/2010GL045404>.
- Krause, T.R., and Whitlock, C., 2013, Climate and vegetation change during the late-glacial/early-Holocene transition inferred from multiple proxy records from Blacktail Pond, Yellowstone National Park, USA: Quaternary Research, v. 79, no. 3, p. 391–402, <https://doi.org/10.1016/j.yqres.2013.01.005>.
- Krause, T.R., and Whitlock, C., 2017, Climatic and non-climatic controls shaping early postglacial conifer history in the northern Greater Yellowstone Ecosystem, USA: Journal of Quaternary Science, v. 32, no. 7, p. 1022–1036, <https://doi.org/10.1002/jqs.2973>.
- Larsen, D.J., Crump, S.E., and Blumm, A., 2020, Alpine glacier resilience and neoglacial fluctuations linked to Holocene snowfall trends in the western United States: Science Advances, v. 6, <https://doi.org/10.1126/sciadv.abc7661>.
- Licciardi, J.M., and Pierce, K.L., 2018, History and dynamics of the Greater Yellowstone glacial system during the last two glaciations: Quaternary Science Reviews, v. 200, p. 1–33, <https://doi.org/10.1016/j.quascirev.2018.08.027>.

- Loewen, M.W., Bindeman, I.N., and Melnik, O.E., 2017, Eruption mechanisms and short duration of large rhyolitic lava flows of Yellowstone: Earth and Planetary Science Letters, v. 458, p. 80–91, <https://doi.org/10.1016/j.epsl.2016.10.034>.
- Lowenstern, J.B., Evans, W.C., and Bergfeld, D., 2005, Diffuse and direct sources of CO<sub>2</sub> from Terrace Spring, a large-volume travertine-forming spring at Yellowstone National Park, in 9th Workshop of the IAVCEI Commission on the Chemistry of Volcanic Gasses, Abstracts: Palermo, Italy, <https://doi.org/10.13140/RG.2.1.1675.3681>.
- Lowenstern, J.B., Bergfeld, D., Evans, W.C., and Hunt, A.G., 2015, Origins of geothermal gasses at Yellowstone: Journal of Volcanology and Geothermal Research, v. 302, p. 87–101, <https://doi.org/10.1016/j.jvolgeores.2015.06.010>.
- Ludwig, K.R., and Paces, J.B., 2002, Uranium-series dating of pedogenic silica and carbonate, Crater Flat, Nevada: Geochimica et Cosmochimica Acta, v. 66, no. 3, p. 487–506, [https://doi.org/10.1016/S0016-7037\(01\)00786-4](https://doi.org/10.1016/S0016-7037(01)00786-4).
- Lundeen, Z., Brunelle, A., Burns, S.J., Polyak, V., and Asmerom, Y., 2013, A speleothem record of Holocene paleoclimate from the northern Wasatch Mountains, southeast Idaho, USA: Quaternary International, v. 310, p. 83–95, <https://doi.org/10.1016/j.quaint.2013.03.018>.
- Luo, L., Capezzuoli, E., Rogerson, M., Vaselli, O., Wen, H., and Lu, Z., 2022, Precipitation of carbonate minerals in travertine-depositing hot springs: Driving forces, microenvironments, and mechanisms: Sedimentary Geology, v. 438, <https://doi.org/10.1016/j.sedgeo.2022.106207>.
- Mancini, A., Frondini, F., Capezzuoli, E., Mejia, E.G., Lezzi, G., Matarazzi, D., Brogi, A., and Swennen, R., 2019, Evaluating the geogenic CO<sub>2</sub> flux from geothermal areas by analyzing Quaternary travertine masses: New data from western central Italy and review of previous CO<sub>2</sub> flux data: Quaternary Science Reviews, v. 215, p. 132–143, <https://doi.org/10.1016/j.quascirev.2019.04.030>.
- Marcott, S.A., Clark, P.U., Shakun, J.D., Brook, E.J., Davis, P.T., and Caffe, M.W., 2019, <sup>10</sup>Be age constraints on latest Pleistocene and Holocene cirque glaciation across the western United States: NPJ Climate and Atmospheric Science, v. 2, <https://doi.org/10.1038/s41612-019-0062-z>.
- McCleskey, R.B., Roth, D.A., Nordstrom, D.K., Hurwitz, S., Holloway, J.M., Bliznik, P.A., Ball, J.W., Repert, D.A., and Hunt, A.G., 2022, Water-Chemistry and Isotope Data for Selected Springs, Geysers, Streams, and Rivers in Yellowstone National Park, Wyoming: U.S. Geological Survey Data Release, <https://doi.org/10.5066/P92XKJU7>.
- McKenzie, W.F., and Truesdell, A.H., 1977, Geothermal reservoir temperatures estimated from the oxygen isotope compositions of dissolved sulfate and water from hot springs and shallow drillholes: Geothermics, v. 5, p. 51–61, [https://doi.org/10.1016/0375-6505\(77\)90008-6](https://doi.org/10.1016/0375-6505(77)90008-6).
- Moran, J.J., Whitmore, L.M., Jay, Z.J., Jennings, R., Beam, J.P., Kreuzer, H.W., and Inskip, W.P., 2017, Dual stable isotopes of CH<sub>4</sub> from Yellowstone hot-springs suggest hydrothermal processes involving magmatic CO<sub>2</sub>: Journal of Volcanology and Geothermal Research, v. 341, p. 187–192, <https://doi.org/10.1016/j.jvolgeores.2017.05.011>.
- Morgan, L.A., Shanks, W.C.P., Pierce, K.L., Iverson, N., Schiller, C.M., Brown, S.R., Zahajka, P., Cartier, R., Cash, R.W., Best, J.L., Whitlock, C., Fritz, S., Benzel, W., Lowers, H., Lovallo, D.A., and Licciardi, J.M., 2023, The dynamic floor of Yellowstone Lake, Wyoming, USA: The last 14 k.y. of hydrothermal explosions, venting, doming, and faulting: Geological Society of America Bulletin, v. 135, p. 547–574, <https://doi.org/10.1130/B36190.1>.
- Muffler, L.J.P., White, D.E., Truesdell, A.H., and Fournier, R.O., 1982a, Geologic Map of Lower Geyser Basin, Yellowstone National Park, Wyoming: U.S. Geological Survey Miscellaneous Investigations Series Map I-1373, scale 1:24,000, <https://doi.org/10.3133/i1373>.
- Muffler, L.J.P., White, D.E., Beeson, M.H., and Truesdell, A.H., 1982b, Geologic Map of Upper Geyser Basin, Yellowstone National Park, Wyoming: U.S. Geological Survey Miscellaneous Investigations Series Map I-1371, scale 1:4800, <https://doi.org/10.3133/i1371>.
- Paces, J.B., Hurwitz, S., Harrison, L.N., and Cullen, J.T., 2022, Sr and U Concentrations and Radiogenic Isotope Compositions (<sup>87</sup>Sr/<sup>86</sup>Sr, <sup>234</sup>U/<sup>238</sup>U) of Thermal Waters, Streamflow, Travertine, and Rock Samples along with U-Th Disequilibrium Ages for Travertine Deposits from Various Locations in Yellowstone National Park, USA: U.S. Geological Survey Data Release, <https://doi.org/10.5066/P9JXP2RO>.
- Pierce, K.L., Adams, K.D., and Sturchio, N.C., 1991, Geologic setting of the Corwin Springs Known Geothermal Resources Area—Mammoth Hot Springs area in and adjacent to Yellowstone National Park, in Sorey, M., ed., Effects of Potential Geothermal Development in the Corwin Springs Known Geothermal Resources Area, Montana, on the Thermal Features of Yellowstone National Park: U.S. Geological Survey Water-Resources Investigations Report 91-4052, <https://doi.org/10.3133/wri914052>.
- Pierce, K.L., Muhs, D.R., Fosberg, M.A., Mahan, S.A., Rosenbaum, J.G., Licciardi, J.M., and Pavich, M.J., 2011, A loess-paleosol record of climate and glacial history over the past two glacial-interglacial cycles (~150 ka), southern Jackson Hole, Wyoming: Quaternary Research, v. 76, p. 119–141, <https://doi.org/10.1016/j.yqres.2011.03.006>.
- Priewisch, A., Crossey, L.J., Karlstrom, K.E., Polyak, V.J., Asmerom, Y., Nereson, A., and Ricketts, J.W., 2014, U-series geochronology of large-volume Quaternary travertine deposits of the southeastern Colorado Plateau: Evaluating episodicity and tectonic and paleohydrologic controls: Geosphere, v. 10, p. 401–423, <https://doi.org/10.1130/GES00946.1>.
- Rahilly, K.E., and Fischer, T.P., 2021, Total diffuse CO<sub>2</sub> flux from Yellowstone caldera incorporating high CO<sub>2</sub> emissions from cold degassing sites: Journal of Volcanology and Geothermal Research, v. 419, <https://doi.org/10.1016/j.jvolgeores.2021.107383>.
- Rye, R.O., and Truesdell, A.H., 2007, The question of recharge to the deep thermal reservoir underlying the geysers and hot springs of Yellowstone National Park, in Morgan, L.A., ed., Integrated Geoscience Studies in the Greater Yellowstone Area—Volcanic, Tectonic, and Hydrothermal Processes in the Yellowstone Geocosystem: U.S. Geological Survey Professional Paper 1717, p. 239–270, <https://doi.org/10.3133/pp1717H>.
- Schiller, C.S., Whitlock, C., and Brown, S., 2022, Holocene geo-ecological evolution of Lower Geyser Basin, Yellowstone National Park (USA): Quaternary Research, v. 105, p. 201–217, <https://doi.org/10.1017/qua.2021.42>.
- Shuman, B.N., and Marsicek, J.P., 2016, The structure of Holocene climate change in mid-latitude North America: Quaternary Science Reviews, v. 141, p. 38–51, <https://doi.org/10.1016/j.quascirev.2016.03.009>.
- Shuman, B.N., and Serravezza, M., 2017, Patterns of hydroclimatic change in the Rocky Mountains and surrounding regions since the Last Glacial Maximum: Quaternary Science Reviews, v. 173, p. 58–77, <https://doi.org/10.1016/j.quascirev.2017.08.012>.
- Stelten, M.E., Thomas, N., Pivarunas, A., and Champion, D., 2023, Spatio-temporal clustering of post-caldera eruptions at Yellowstone caldera: Implications for volcanic hazards and pre-eruptive magma reservoir configuration: Bulletin of Volcanology, v. 85, <https://doi.org/10.1007/s00445-023-01665-w>.
- Sturchio, N.C., Keith, T.E.C., and Muehlenbachs, K., 1990, Oxygen and carbon isotope ratios of hydrothermal minerals from Yellowstone drill cores: Journal of Volcanology and Geothermal Research, v. 40, p. 23–37, [https://doi.org/10.1016/0377-0273\(90\)90104-N](https://doi.org/10.1016/0377-0273(90)90104-N).
- Sturchio, N.C., Pierce, K.L., Murrell, M.T., and Sorey, M.L., 1994, Uranium-series ages of travertines and timing of the last glaciation in the northern Yellowstone area, Wyoming-Montana: Quaternary Research, v. 41, no. 3, p. 265–277, <https://doi.org/10.1006/qres.1994.1030>.
- U.S. Geological Survey 3D Elevation Program, 2022, 1 m LiDAR point cloud and DEM data Yellowstone National Park 2020 (accessed through The National Map: <https://apps.nationalmap.gov/lidar-explorer/#/>).
- Uysal, I.T., Feng, Y., Zhao, J.-X., Isik, V., Nuriel, P., and Goding, S.D., 2009, Hydrothermal CO<sub>2</sub> degassing in seismically active zones during the late Quaternary: Chemical Geology, v. 265, p. 442–454, <https://doi.org/10.1016/j.chemgeo.2009.05.011>.
- Vazquez, J.A., and Reid, M.R., 2002, Time scales of magma storage and differentiation of voluminous high-silica rhyolites at Yellowstone caldera, Wyoming: Contributions to Mineralogy and Petrology, v. 144, p. 274–285, <https://doi.org/10.1007/s00410-002-0400-7>.
- Waldrop, H.A., 1975, Surficial Geologic Map of the Old Faithful Quadrangle, Yellowstone National Park, Wyoming: U.S. Geological Survey Miscellaneous Investigations Series Map I-649, scale 1:62,500, <https://doi.org/10.3133/i649>.
- Waldrop, H.A., and Pierce, K.L., 1975, Surficial Geologic Map of the Madison Junction Quadrangle Yellowstone National Park, Wyoming: U.S. Geological Survey Miscellaneous Investigation Series Map I-651, scale 1:62,500, <https://doi.org/10.3133/i651>.
- Wang, P., Du, Y., Yu, W., Algeo, T.J., Zhou, Q., Xu, Y., Qi, L., Yuan, L., and Pan, W., 2020, The chemical index of alteration (CIA) as a proxy for climate change during glacial-interglacial transitions in Earth history: Earth-Science Reviews, v. 201, <https://doi.org/10.1016/j.earscirev.2019.103032>.
- Watts, K.E., Bindeman, I.N., and Schmitt, A.K., 2012, Crystal scale anatomy of a dying supervolcano: An isotope and geochronology study of individual phenocrysts from voluminous rhyolites of the Yellowstone caldera: Contributions to Mineralogy and Petrology, v. 164, p. 45–67, <https://doi.org/10.1007/s00410-012-0724-x>.
- Werner, C., and Brantley, S., 2003, CO<sub>2</sub> emissions from the Yellowstone volcanic system: Geochemistry, Geophysics, Geosystems, v. 4, no. 7, <https://doi.org/10.1029/2002GC000473>.
- White, D.E., Fournier, R.O., Muffler, L.P.J., and Truesdell, A.H., 1975, Physical Results of Research Drilling in Thermal Areas of Yellowstone National Park, Wyoming: U.S. Geological Survey Professional Paper 892, 70 p., <https://doi.org/10.3133/pp892>.
- Whitlock, C., 1993, Postglacial vegetation and climate of Grand Teton and southern Yellowstone National Parks: Ecological Monographs, v. 63, p. 173–198, <https://doi.org/10.2307/2937179>.
- Whitlock, C., Dean, W., Rosenbaum, J., Stevens, L., Fritz, S., Bracht, B., and Power, M., 2008, A 2650-year-long record of environmental change from northern Yellowstone National Park based on a comparison of multiple proxy data: Quaternary International, v. 188, p. 126–138, <https://doi.org/10.1016/j.quaint.2007.06.005>.
- Whitlock, C., Dean, W.E., Fritz, S.C., Stevens, L.R., Stone, J.R., Power, M.J., Rosenbaum, J.R., Pierce, K.L., and Bracht-Flyer, B., 2012, Holocene seasonal variability inferred from multiple proxy records from Crevice Lake, Yellowstone National Park, USA: Palaeogeography, Palaeoclimatology, Palaeoecology, v. 331–332, p. 90–103, <https://doi.org/10.1016/j.palaeo.2012.03.001>.

SCIENCE EDITOR: BRAD SINGER  
ASSOCIATE EDITOR: ALESSANDRO ZANAZZI

MANUSCRIPT RECEIVED 7 SEPTEMBER 2023  
REVISED MANUSCRIPT RECEIVED 31 OCTOBER 2023  
MANUSCRIPT ACCEPTED 20 DECEMBER 2023